Published in final edited form as:

Exp Neurol. 2016 September ; 283(Pt A): 413–427. doi:10.1016/j.expneurol.2016.06.002.

Cutaneous tissue damage induces long-lasting nociceptive sensitization and regulation of cellular stress- and nerve injury-associated genes in sensory neurons

Kristofer K. Rau[a,b,c,1], **Caitlin E. Hill**[d,e,1], **Benjamin J. Harrison**[b,c,f], **Gayathri Venkat**[b,c], **Heidi M. Koenig**[a], **Sarah B. Cook**[d], **Alexander G. Rabchevsky**[g,h], **Bradley K. Taylor**[g], **Tsonwin Hai**[i], and **Jeffrey C. Petruska**[b,c,f,j,*]

[a]University of Louisville, Department of Anesthesiology, Louisville, KY, United States

[b]University of Louisville, Department of Anatomical Sciences and Neurobiology, Louisville, KY, United States

[c]University of Louisville, KY Spinal Cord Injury Research Center, Louisville, KY, United States

[d]Burke Medical Research Institute, White Plains, NY, United States

[e]Weill Cornell Medicine, Feil Family Brain and Mind Research Institute, New York, NY, United States

[f]University of Louisville, KY Biomedical Research Infrastructure Network (KBRIN), Louisville, KY, United States

[g]University of Kentucky, Department of Physiology, Lexington, KY, United States

[h]University of Kentucky, Spinal Cord and Brain Injury Research Center, Lexington, KY, United States

[i]Ohio State University, Department of Molecular and Cellular Biochemistry, Columbus, OH, United States

[j]University of Louisville, Department of Neurological Surgery, Louisville, KY, United States

Abstract

Tissue damage is one of the major etiological factors in the emergence of chronic/persistent pain, although mechanisms remain enigmatic. Using incision of the back skin of adult rats as a model for tissue damage, we observed sensitization in a nociceptive reflex enduring to 28 days post-incision (DPI). To determine if the enduring behavioral changes corresponded with a long-term impact of tissue damage on sensory neurons, we examined the temporal expression profile of injury-regulated genes and the electrophysiological properties of traced dorsal root ganglion (DRG) sensory neurons. The mRNA for the injury/stress-hub gene Activating Transcription Factor

[*]Corresponding author at: University of Louisville, Department of Anatomical Sciences and Neurobiology, 511 South Floyd Street, MDR Building 1st floor, Louisville, KY 40292, United States. j.petruska@louisville.edu (J.C. Petruska).

[1]Contributed equally.

Conflict of interest

The authors have declared that no conflict of interest exists.

3 (ATF3) was upregulated and peaked within 4 DPI, after which levels declined but remained significantly elevated out to 28 DPI, a time when the initial incision appears healed and tissue-inflammation largely resolved. Accordingly, stereological image analysis indicated that some neurons expressed ATF3 only transiently (mostly medium-large neurons), while in others it was sustained (mostly small neurons), suggesting cell-type-specific responses. In retrogradely-traced ATF3-expressing neurons, Calcium/calmodulin-dependent protein kinase type IV (CAMK4) protein levels and isolectin-B4 (IB4)-binding were suppressed whereas Growth Associated Protein-43 (GAP-43) and Neuropeptide Y (NPY) protein levels were enhanced. Electrophysiological recordings from DiI-traced sensory neurons 28 DPI showed a significant sensitization limited to ATF3-expressing neurons. Thus, ATF3 expression is revealed as a strong predictor of single cells displaying enduring pain-related electro-physiological properties. The cellular injury/stress response induced in sensory neurons by tissue damage and indicated by ATF3 expression is positioned to contribute to pain which can occur after tissue damage.

Keywords

Dorsal root ganglion; Pain; Nociceptor; Tissue damage; Cell stress

1. Introduction

A wide variety of tissue damage, including surgery and what could be considered minor damage, can lead to painful conditions that remain long after the wound has apparently healed. Commonly-performed surgical procedures often carry persistent post-surgical pain (e.g., Kehlet et al., 2006; Borsook et al., 2013), and many of the most difficult-to-treat pain conditions arise after tissue damage (e.g., de Mos et al., 2009; Goebel, 2011; Huge et al., 2011). It is clear that peripheral sensory neurons, with cell bodies located in the dorsal root ganglia (DRGs), play an important role in the development of this persistent pain (Woolf and Salter, 2000; Gold and Flake, 2005; Ellis and Bennett, 2013).

Experimental models of chronic/persistent pain (C/PP) using nerve injury have identified changes in DRG neuron gene expression and electrophysiological properties, some of which are long-lasting and may contribute to C/PP (e.g., Van der Zee et al., 1989; Chong et al., 1992; Costigan et al., 2002; Ma et al., 2003). Experimental models of tissue damage have revealed important and tractable mechanisms of short-term hyperalgesia and pain, but have been less revealing of feasible mechanisms of persistent pain (e.g., Brennan et al., 1996; Perkins and Kehlet, 2000; Pogatzki et al., 2002a, 2002b; Buvanendran et al., 2004).

Identifying important biological responses in sensory neurons which may contribute to C/PP is made more difficult in tissue damage models because these generate mixed populations. Some neurons are directly affected by the damage and others are indirectly affected by subsequent tissue inflammation, etc., yet both have a combined influence on the sensory system. Also, many models use animals that have endogenous analgesic mechanisms which can mask persistent sensory pathologies (Solway et al., 2011). Further, many experimental approaches screen for C/PP-like states using withdrawal reflexes which may not detect changes in animals which could nonetheless represent important phenomena for

understanding the human condition (Vierck and Yezierski, 2015). Combined, these issues may have prevented the detection of underlying nervous system responses in animal models which may contribute to C/PP-like states in humans.

In an effort to identify additional potential models of tissue damage in which C/PP-related conditions might be detectible in animals, we used incision of the back hairy skin of adult rats. We examined whether skin incision resulted in enduring behavioral changes using the cutaneous trunci muscle reflex (CTMr; Petruska et al., 2014). This nociceptive reflex system differs in important ways from the commonly-used hindlimb and tail withdrawal reflexes. Notably, the strength of the CTMr lies in quantifying the magnitude and duration of the response whereas hindlimb withdrawal reflexes are better-suited than the CTMr for quantifying threshold changes. The CTMr system revealed a sensitization induced by incision that persisted beyond resolution of tissue-inflammation.

In an effort to identify additional potential mechanisms which might contribute to C/PP we moved away from the conceptual framework of tissue-inflammation. Instead, we considered that tissue-damage likely injures sensory axons and induces a cellular stress/injury response in sensory neurons although their axons remain in contact with their target tissue. This framework is understudied in relation to pain mechanisms after tissue damage, but has been well-considered in nerve injury-related pain. We previously determined that some of the same gene regulation which occurs after peripheral nerve injury also occurs after skin incision, including de novo expression of Activating Transcription Factor 3 (ATF3; Hill et al., 2010) and other stress/injury/regeneration-associated genes in sensory neurons innervating the incision-associated skin.

In the current study our findings suggest that a cellular stress/injury response may persist in many (but not all) incision-associated sensory neurons. Further, only neurons which express ATF3 also display persistent electrophysiological sensitization. This suggests that ATF3 and the cellular stress/injury response it represents may effectively segregate a mixed population of neurons innervating the peri-wound skin. Such prolonged expression of a cellular stress/injury response and sensitization could represent an additional mechanism which contributes to persistent sensory pathologies after tissue damage.

2. Material and methods

2.1. General animal care

Animal care and procedures were carried out at the University of Louisville, and were in accord with approved IACUC protocols. Sixty-six age-matched adult female Sprague-Dawley rats (180–200 g; Taconic, Indianapolis, Indiana) were used for these studies [Real-time quantitative PCR (RT-qPCR): n = 20; immunohistochemistry: n = 26; electrophysiology: n = 12; behavior: n = 8]. For all surgeries, rats were anesthetized with ketamine/xylazine (i.p. injection; 80 mg/kg ketamine; 10 mg/kg xylazine) and body temperature was monitored and maintained at 36 °C throughout the surgeries which lasted 20–30 min. Puralube ointment (Dechra) was used to protect the rat's eyes during surgery. Following surgery, rats were given lactated ringer's solution (5 cm^3, i.p.) to prevent dehydration, and gentamycin (Gentafuse; 0.1 cm^3, i.m., every other day for 7 days) to

prevent infection. Rats were monitored daily and housed individually throughout the experiment.

2.2. Surgical procedures

Incisions involved cutting the full thickness of both the hairy skin and the underlying attached cutaneous trunci muscle. Following incision, the skin was closed with Ethilon nylon suture (5-0, Ethicon), and coated with Bacitracin antibiotic ointment (Actavis) to prevent infection.

2.2.1. Experimental incision—The experimental incision used to examine the molecular, histological and physiological changes in the DRG neurons, as well as behavioral changes in the CTMr, was made on the *left side* of the rats. It was located 1 cm lateral to the vertebral column and extended parallel to the vertebral column for 3 cm (including approximately the T7–12 dermatomes). The location of the incision ensured that the dorsal cutaneous nerves were not damaged by the incision. See Fig. 1.

2.2.2. Tracer incision—For rats in which DRGs were to be examined histologically or electrophysiologically, an additional skin incision was made, *on the right side*, seven days prior to the experimental skin incision to allow for tracer injection and transport. This skin incision to enable tracer injection was placed on the right side to prevent damage to the axons of interest on the left side. Following incision on the right side, the skin was reflected to expose the underside of the contralateral (left) skin. 0.5% DiI (1,1′-dilinoleyl-3,3,3′,3′-tetramethylindocarbocyanine perchlorate; 5 mg FastDiI dissolved in 1 ml methanol; Invitrogen) was injected into the subdermal layer using a Hamilton syringe. Ten injections of 1 μl each, were used to target the terminal field as described previously (Jiang et al., 2006; Rau et al., 2007). The Experimental Incision was approximately 5 mm distal *to*, and extended at least two dermatomes rostral and caudal *from* the DiI injected region (see Fig. 1). Preliminary studies indicated that this method maximized the percentage of DiI-labeled cells that were injured by incision, as indicated by ATF3/DiI co-localization.

2.3. Behavioral analysis

The CTMr was used to assess pain-related behavioral changes after incision. Use of this reflex as a model system has been described in detail previously (Petruska et al., 2014). Prior to recording, animals were sedated with pentobarbital (35 mg/kg), to which the CTMr is highly resistant. A standardized matrix of dots (5 mm apart) was drawn on the back skin (Fig. 2A). Calibrated Adson forceps were used to apply a standardized noxious mechanical stimulus to select points on the left side of the animal, adjacent to the incision site (or equivalent in non-incised animals). Adson forceps (dull tips) were used as opposed to #5 Dumont forceps (sharp tips). This prevented dual-activation of the CTMr which occurs with Dumont forceps — first by “pin-prick” stimulus when the sharp tips contact the skin, and second by the pinch. Use of the Adson forceps significantly reduced the variability in the reflex data. Video capture and semi-automated biokinematic processing of the reflex movement was acquired using MaxTRAQ software (Innovision Systems). Video motion data was compiled using a custom plug-in for Microsoft Excel.

2.4. Sample generation

It is important to note for the following sections that the thoracic DRG used to assess the effects of skin incision do not contain neurons innervating the underlying CTM. The sensory innervation of the thin CTM that is inserted along the back skin differs from the overlying skin – it arises from DRG in the brachial region (see Petruska et al., 2014).

The range of time points examined (4–28 days post-incision) encompasses both sub-acute time points in which inflammation-related mechanisms are known to be at play, and later times points when inflammation has typically resolved (≥ 10–14 days). This range also encompasses the majority of the wound healing process. The skin is closed (surface wound contraction) to the point where sutures and/or staples can be removed by 7–10 days. Numerous prior studies using the same back skin-incision model indicate that the majority of injury conditions (e.g., hypoxia) and the microscale repair processes (e.g., vascular remodeling) are completed between 14 and 21 days after incision and closure (e.g., Lokmic et al., 2006; Soybir et al., 2012; Gong et al., 2013; Kang et al., 2013; Farahpour et al., 2015), though other aspects take longer. For example, the vascular volume density and vascular proliferation return to non-injured levels within 10–14 days after injury, although refined remodeling continues for up to 16 weeks (Lokmic et al., 2006). By day 21 the stiffness of healed skin tissue recovers to 97% of its pre-wounded state and the tensile strength approaches 50% (Chao et al., 2013).

2.4.1. Tissue for RT-qPCR analysis—Rats received an experimental incision (n = 16) and tissue was collected 4, 7, 14 or 28 days post-incision (DPI: n = 4/time point). A control group of rats received no experimental incision (n = 4). For tissue collection, rats were euthanized with an overdose of pentobarbital and transcardially exsanguinated with heparinized phosphate buffered saline (PBS; pH 7.4). This was followed by 33% vol/vol RNAlater (Qiagen) in heparinized PBS to help preserve the RNA. Three adjacent DRGs with projections to the incision site (typically T10–T12; innervation of incision site confirmed by gross-anatomical dissection) were collected, pooled together, and placed in 100% RNAlater overnight at 4 °C and then stored at −80 °C until RNA isolation.

2.4.2. Tissue for histological analysis—A group of rats (n = 6) received a tracer incision and an injection of 0.5% DiI into the future site of the experimental incision. Seven days later, the time required for the injected tracer to be transported back to the cell-bodies in the DRG, half of the rats received the experimental incision (n = 3). The remaining rats (n = 3) served as no skin-incision controls. Seven days after the experimental incision, tissue was collected (see below). Tissue from this group of rats was used to examine the neurochemical response of DRG neurons innervating the site of injection/incision.

A second group of rats received an experimental incision (without tracer injection) and tissue was collected 4, 7, 14 or 28 days post-incision (DPI: n = 4/time point). An additional cohort of rats in this group received no skin-incision (n = 4) and served as no skin-incision controls. Tissue from these rats was assessed using stereology.

For tissue collection for histology, rats were euthanized with an overdose of pentobarbital and transcardially exsanguinated with heparinized PBS (pH 7.4) followed by 4%

paraformaldehyde (PFA) in PBS. DRGs with anatomically-confirmed projections to the site of skin incision were collected, post-fixed in 4% PFA overnight and cryopreserved in 30% sucrose-PBS prior to embedding in OCT matrix.

2.4.3. Tissue for electrophysiological studies—Rats (n = 12) received a tracer incision and injection of 0.5% DiI into the future site of the experimental incision. Seven days later, half of the rats received an experimental incision (n = 6). The remaining rats (n = 6) served as no experimental skin-incision controls. Twenty-eight days post skin incision, rats were terminally euthanized and exsanguinated as described above (without PFA). DRGs with anatomically-confirmed projections to the DiI-labeled zone were retrieved and processed for patch clamping and subsequent immunohistochemistry.

2.5. RNA isolation

To isolate RNA from the DRGs, samples were placed on ice and 350 μl RLT lysis buffer (Qiagen) and 2-mercaptoethanol was added. Tissue was homogenized for 1 min using a motorized dual Teflon glass homogenizer (Kontes). RNA was extracted using the RNeasy plus micro kit (Qiagen) as per manufacturer's protocol. Genomic DNA was removed using the DNA eliminator affinity spin column and RNA was purified by affinity purification using RNA spin columns. Samples were eluted in 14 μl of nuclease free water. RNA integrity was assessed by UV spectrometry and the Bioanalyzer (Agilent Technologies). RNA samples with 260 nm/280 nm ratios above 1.9 and 260 nm/230 nm ratios and RNA integrity numbers above 1.8 were used for RT-qPCR.

2.6. RT-qPCR

RT-qPCR was used to quantify the expression of genes within DRGs following skin incision. We examined ATF3, Growth Associated Protein-43 (GAP-43) and Neuropeptide Y (NPY) within the DRGs, which are all known to be upregulated after nerve injury, and are involved in neural plasticity (Van der Zee et al., 1989; Tsujino et al., 2000; Tsai et al., 2007). We previously reported an acute increase in ATF3 and GAP-43 in DRGs following skin incision (Hill et al., 2010).

cDNA was generated from the RNA samples using the Quantitect first strand synthesis kit (Qiagen) according to the manufacturer's protocol. For each PCR reaction, 5 ng of cDNA template was used. Samples were run in triplicate, and control reactions (without template) were included with every amplification run. SYBR green RT-qPCR was carried out using a Rotorgene real time PCR detection instrument (Corbett Research, now Qiagen, Inc.). Relative fold-changes of RNA were calculated by the ΔΔCT method using GAPDH as the stable internal reference gene. Small differences in RT-qPCR reaction efficiency between primer sets were accounted for using the standard curve quantification methods. Primer details are shown in Table 1.

2.7. Cryosectioning

DRGs were embedded in OCT compound and cryostat sectioned at 14 μm. For DiI-labeled DRG, serial sections were mounted across 6 slides. This yielded individual slides with sections sampling the DRG every 84 μm. For studies using non-DiI-traced DRGs, serial

sections were mounted on 8 slides, such that there was at least 112 μm between each section on a given slide. The spacing between sections ensured that no single neuron could be counted more than once on any given slide.

2.8. Histochemistry

In order to determine if skin incision induced an injury-like response in sensory neurons we assessed the expression of markers known to be affected by nerve-injury. ATF3, GAP-43 and NPY are upregulated after nerve injury. We also assessed the expression of two other markers in the DRG whose expression decreases in response to nerve injury —calcium/calmodulin-dependent protein kinase type IV (CAMK4; Ji et al., 1996) and isolectin B4 (IB4)-binding (Bennett et al., 1998). Reagents used were: ATF3 (Santa Cruz Biotechnology, rabbit polyclonal, Catalog # SC-188), GAP-43 (EnCor Biotech. Inc., chicken polyclonal, Catalog # CPCA-GAP-43), NPY (Neuromics, Guinea pig polyclonal, Catalog # GP14017), CAMK4 (BD Biosciences, mouse monoclonal, Catalog # 610275), Neuronal Nuclei (NeuN; Millipore, mouse monoclonal, Catalog # MAB377), and IB4-binding (Invitrogen, lectin IB4-Alexa-488, Catalog # I21411). All primary antibodies were used at 1:1000 and the lectin at 1:100. Appropriate Alexa-conjugated secondary antibodies (Invitrogen, Alexa-350 or Alexa-488) were used at 1:100 for ATF3, NPY, CAMK4, and NeuN staining. Biotin-conjugated goat-anti-mouse (Jackson ImmunoResearch) was used for GAP-43 immunohistochemistry and visualized as described below.

Sections were blocked with 3.3% normal goat serum, 0.4% Triton-X 100, and PBS for 1 h to prevent non-specific binding. All wash steps following antibody application used this same blocking solution. Primary antibodies for ATF3 and one of the other protein markers were applied overnight, rinsed the next morning, and appropriate species-specific secondary antibodies were then applied for 3 h. Detection of GAP-43' involved additional amplifications steps, in which the secondary antibody step was followed by sequential applications of Avidin-Biotin Complex reagent (Vectastain ABC kit, Vector Labs), biotinylated tyramide signal amplification reagent (Molecular Probes TSA-biotin, Invitrogen), and Dylight-488 conjugated to Steptavidin (1:100; Jackson ImmunoResearch). Controls included performing a dilution series of primary antibody, and omission of individual steps (i.e. primary antibody, secondary antibody, amplification). For some sections, Hoechst dye (1:1000) was applied after incubation of the secondary antibodies to visualize all nuclei. Immunoreactivity is defined as antigen-like.

2.9. Microscopy and image analysis

Two different sets of DRG sections were used to make two separate assessments of the neurochemical response of sensory neurons to incision of the skin they innervated. One approach used stereological methods to quantify the number of ATF3-expressing neurons in the DRG. The other approach assessed the relative intensity of four different injury-related markers in retrogradely-traced neurons. Both methods also assessed the size distribution of the quantified neurons. All procedures were carried out by experimenters blinded to the treatment group.

2.9.1. Stereological quantification of ATF3 expression—Tissue sections were examined on an inverted Zeiss 200 M microscope equipped with digital image acquisition and StereoInvestigator software (MicrobrightField, Inc., Williston, VT). StereoInvestigator was used to quantify the number of neurons expressing specific markers as previously described (Hill et al., 2010), and also characterize the neurons according to size. For each DRG, every 4th tissue section was traced at 10× magnification using DAPI visualization to define neurons and subsequently quantified at 63×.

2.9.1.1. Number of ATF3$^+$ neurons: Sections were immunolabeled as described above to simultaneously visualize ATF3 and GAP-43 proteins. The number of ATF3$^+$/GAP-43$^+$ and ATF3$^+$/GAP-43$^-$ neurons within the DRGs was quantified in tissue samples from skin-incision rats (4, 7, 14 and 28 days post-skin-incision) as well as non-skin-incision rats (n = 4/condition). The optical fractionator function was used to õdetermine the number of neurons that expressed ATF3 and classify them based on whether or not they also expressed GAP-43, a second marker of neuronal injury (counting frame = 100 μm × 100 μm; grid size = 200 μm × 200 μm).

2.9.1.2. Somal size of ATF3$^+$ neurons: The volume of the ATF3$^+$ neurons (GAP-43$^+$ and GAP-43$^-$), initially identified with the optical fractionator function, were subsequently quantified using the nucleator function.

2.9.2. Relative expression intensity of injury-related markers—We also determined the relative staining intensity of GAP-43, NPY, CAMK4 and IB4-binding for DiI-labeled neurons. Images were acquired using a Nikon TiE automated inverted microscope with a Digital Sight DS-Ri1 Digital Camera and Nikon Elements BR software and analyzed using methods similar to those previously described (Burgess et al., 2010). Four to 8 sections per animal were used for imaging. Individual cells to be quantified were identified and manually outlined. Cells were included if they had a visible nucleus (indicated by ATF3 and/or NeuN) and were DiI$^+$. For DRG serving incised skin (Incision group), only neurons with both DiI and ATF3 were counted (n = 1590). For DRG serving non-incised skin (Control group), all DiI-labeled cells were counted (n = 2603 cells).

Background corrections were used to normalize staining intensities across slides and groups. First, background-subtraction was performed on a per-section basis. A region of each section (about the size of 3 neurons) with no staining was selected. This was usually in the ventral root, and manual comparisons were made to ensure this region had the lowest-intensity of the section. The mean intensity value of this “background” region was then calculated and this was subtracted from the raw intensity values of all neurons in that section.

Because the slide is the fundamental unit of histological processing, the range of background-corrected intensity values for each channel was normalized on a per-slide basis according to the equation:

$$\text{neuron mean intensity} = [(\text{“Raw cellular- mean- intensity”} - \text{“minimum- intensity”}) * (100/(\text{“maximum- intensity”} - \text{“minimum- i}$$

For this, “minimum-intensity” is the mean somal intensity of the neuron with the weakest staining for GAP-43, NPY, CAMK4 or IB4-binding, and “maximum-intensity” is the mean somal intensity of the neuron with the strongest staining for GAP-43, NPY, CAMK4 or IB4-binding. Thus, the raw mean-intensity value (the mean intensity of the entire somal area) for each neuron was converted to a percentage value, with the weakest-labeled-neuron defining 0%, and the strongest-labeled-neuron defining 100%. This normalizes any slide-to-slide variation inherent in the procedures. This approach of background-correction and normalization provides an indication of relative intensity without making any claims about the positivity/negativity of expression for any given neuron.

The size of each counted cell was calculated as the average between the minimum and maximum cell diameters. Based on the average diameter of the soma, DRG neurons were classified as either small (<30 μm), medium (30–45 μm) or large (>45 μm) for subsequent analysis.

2.10. DRG dissociations for electrophysiology

DRGs were isolated, dissociated and plated as previously described (Petruska et al., 2000, 2002). DRGs were digested enzymatically with dispase (neutral protease, 5 mg/ml; Boehringer Mannheim) and collagenase (type 1, 2 mg/ml; Sigma) in Tyrode’s solution for 90 min (35 °C). The DRGs were gently triturated every 30 min to dissociate the cells. Following enzymatic treatment and dissociation, cells were pelleted by centrifugation (800 rpm, 3 min), resuspended in fresh Tyrode’s solution and plated onto poly-L-lysine (Sigma)-coated dishes. Prior to recording, dishes were kept in an aerated holding bath for at least 2 h. All recordings were made within 10 h of DRG retrieval from the animal, a time frame prior to translation of ATF3 (Rau et al., 2014) – i.e., the ATF3 expression in dissociated/recorded neurons we described was due to the skin incision and not to the dissociation process.

2.11. Electrophysiology

Whole-cell patch recording was used to determine the electrophysiological properties of individually isolated DiI-labeled neurons (i.e., those that had projected to the site of the skin incision). In total 55 DRG neurons were assessed [skin-incision (incision group): n = 23; no-skin incision (control group): n = 32]. Electrophysiology was performed as previously described in detail (Petruska et al., 2000, 2002). Recordings were performed with a Scientifica SliceScope Pro system. Electrodes were prepared (2–4 MΩ) from glass pipettes using a horizontal puller (Sutter model P1000). Electrophysiology solutions: Extracellular (Tyrode’s) solution consisted of 140 mM NaCl, 4 mM KCl, 2 mM $MgCl_2$, 2 mM $CaCl_2$, 10 mM glucose, and 10 mM HEPES, adjusted to pH 7.4 with NaOH. The recording electrodes were filled with 120 mM KCl, 5 mM Na_2-ATP, 0.4 mM Na_2-GTP, 5 mM EGTA, 2.25 mM $CaCl_2$, 5 mM $MgCl_2$, and 20 mM HEPES, adjusted to pH 7.4 with KOH; osmolarity was ~315–325 mOsm.

DiI-labeled neurons were identified by briefly illuminating the dish using epifluorescence microscopy (total exposure of field <1 min). Once identified, whole cell recordings were made with an Axoclamp 2B (Molecular Devices). Stimuli were controlled and digital records captured with pClamp10 software and a Digidata 1440 (Molecular Devices). Series

resistance (R_S) was compensated 50–70%. Whole cell resistance (R_M) and capacitance was assessed by pClamp software from voltage transients associated with small step commands (10 mV). All experiments were conducted at room temperature. Only cells having a resting membrane potential (RMP) of −40 to −70 mV were included in this study.

After obtaining and stabilizing individual DRG neurons under whole cell patch clamp in voltage-clamp mode, cells were brought into current-clamp mode to assess changes in membrane potential. In order to assess cellular excitability we determined rheobase (the minimum current needed for action potential generation). In order to assess cellular responsiveness we determined action potential frequency (mean, maximum and instantaneous) in response to standardized depolarizing current steps. In order to determine if there were changes to the currents underlying action potentials, we measured certain parameters. Action potentials were evoked through a 1 ms, 2 nA current step. The average of ten action potentials was used to determine after-hyperpolarization duration of 80% recovery to baseline (Djouhri et al., 1998), and after-hyperpolarization amplitude (decrease in voltage from RMP to the lowest point of the after-hyperpolarization). After-hyperpolarization parameters can affect the firing frequency of the neuron. Action potential threshold and action potential duration at threshold (APDt) were determined at rheobase on top of 500-ms square pulses increased in 50-pA increments every 2 s (and further refined using 5-pA increments). Threshold was defined as the membrane potential at which the rate of voltage change exceeded 5 V/s, and was determined using the first derivative of the action potential waveform (Davidson et al., 2014). Action potential threshold dictates how easily the neurons can be induced to fire. APDt was measured as the time from the first upward deflection of the action potential waveform to its return to the threshold membrane potential. APDt can influence maximum firing frequency. Numbers of evoked action potentials and peak instantaneous frequency were determined using increasing voltage steps (1-second stimulus duration, 10-second interstimulus duration; stimuli were increased in 50-pA steps over 20 sweeps, resulting in evoked current recordings from 50 to 1000 pA). All measurements of electrophysiological recordings were performed using Clampfit analysis software.

Only one cell was recorded per dish. After recording was completed, the recorded cell was marked for later identification by physically marking the cell location on the underside of the plastic culture dish and capturing a digital image with a Scientifica monochrome camera using SCIght 2.0 image capture software. The bath solution was replaced with 4% PFA in PBS for 10 min and then repeatedly rinsed and replaced with a 100% PBS solution. Cells were stored at 4 °C until the immunolabeling procedures were performed. Immunocytochemistry procedures to examine ATF3 expression within individual DRG neurons in dishes following electrophysiological recordings were performed as described above for tissue sections. Recorded/immunolabeled cells were then located and characterized as described in the Microscopy and Image Analysis section above. Eighty-four percent of recorded neurons were subsequently recovered and analyzed by immunohistochemistry. The electrophysiological data for those neurons not recovered for immunohistochemistry are included in the “all” group data listed in Fig. 6.

2.12. Statistical analyses

Statistical analyses were performed using SigmaPlot/SigmaStat (Systat Software, San Jose, CA, USA). First-pass analysis to examine differences between the skin-incised and control groups for all assessments was done using one-way analysis of variance (ANOVA), and was followed by pair-wise comparisons (Student-Newman-Keuls). ANOVA on ranks was used to compare distributions that failed normality testing (common for gene expression that is "off-to-on" as it is for ATF3 expression), and was followed either by the Kolmogorov-Smirnov test or Holm-Sidak method. For some comparisons, other methods were also used and are indicated in the text and/or figure legends.

For image analysis, some comparisons synthesized the data from individual neurons into a representative value for the animal. This value was then used as the single-animal-value for comparisons in which the degrees of freedom equaled the number of animals and the groups were compared (i.e., skin-incised vs. control). For other comparisons, such as the relative-intensity of the various markers in individual cells, the degrees of freedom equaled the number of cells. Where degrees of freedom equal number of cells, we have ensured (by ANOVA) that the number of cells/animal are statistically equivalent in terms of 1) the number of cells, and 2) their size/frequency distribution. This reduces the opportunity for data from any given animal to bias the overall data. For electrophysiological comparisons, one-way ANOVA with Dunnett's post-hoc *t*-test was used to compare properties between the skin-incised and control groups as a whole, as well as to compare the groups using neuron populations broken up based on ATF3 expression (i.e., $ATF3^+$ cells in skin-incised group vs. control group and $ATF3^-$ cells in skin-incised group vs. control group). Analysis of potential differences in electrophysiological properties between $ATF3^+$ and $ATF3^-$ neurons was performed using the binomial proportion test (Siegel and Castellan, 1988). Differences were considered to be statistically significant if $p < 0.05$. Data is presented as mean ± standard error.

3. Results

3.1. Sensitization in a nociceptive reflex

The pain field in general, both clinical and basic science, recognizes that most animal models of the human chronic neuropathic pain condition are limited in many ways, but are nonetheless necessary and are still useful (Mogil et al., 2010; Berge, 2011). Skin incision serves as a model of post-surgical pain (Brennan et al., 1996). Skin incision can also serve as a relatively simple model of tissue damage generally. Chronic pain after apparently-minor tissue damage remains one of the most enigmatic conditions and is in great need of new insights regarding potential mechanisms (Kehlet et al., 2006; Arroyo-Novoa et al., 2009).

Just as many models are limited but useful, so too are the assessment tools. The most frequently-used nociceptive behavioral tests for pain-related sensitization are the Hargreaves test (for thermal sensitivity) and the von Frey test (for mechanical sensitivity), both of which are performed on the hindpaws. These tests are strong for determining the latency/threshold for reflex activation, but are generally weak for quantifying amplitude or duration of response. Although highly useful for many purposes, these tests may give false-negative

results if the characteristics being studied affect something other than response latency/threshold. Sensory neuron mechanisms of persistent pain might affect the amplitude and duration of nociceptive responses, either in addition to or instead of affecting response-threshold. We therefore used a different reflex system, the CTMr (Fig. 2A; Petruska et al., 2014), which has strength for quantifying the characteristics for which Hargreaves and von Frey are weak.

The CTMr is a puckering of the back skin induced by noxious stimuli. The CTMr was induced by applying standardized noxious pinch to peri-incisional skin (on left side) and to the corresponding right-side non-incised skin, and equivalent areas in control animals which received no incision. Reflex parameters were assessed by measuring the distance between dots placed on the back skin and their movement over time after stimulation. We compared the biokinematic characteristics of the CTMr between non-incision animals and those 28 days after experimental incision. We found that the reflex magnitude, represented by the maximum contraction distance and by the contraction speed, was significantly increased (Fig. 2B, C) after peri-incisional stimulation. Further, the response duration, measured as the relaxation time (time from stimulus-end to return to 80% of pre-stimulus dot-distance; Fig. 2D) was increased after peri-incisional stimulation. Given the common characteristic of spontaneous pain in many neuropathic pain conditions, it is worth noting that we did not observe any spontaneous CTMr contractions, including on the incisional side, though our recording sessions were not ideally-designed for this assessment. These data suggest that there is a prolonged sensitization of a nociceptive-specific reflex, at least out to 28 days post-incision.

3.2. Temporal expression of injury/stress-associated genes in the DRG following skin incision

Genes associated with cellular injury/stress, including regeneration-associated genes (RAGs), are regulated in neurons following nerve injury and some are associated with neuropathic pain. ATF3, a major hub-regulator of the cellular injury/stress response, is induced de novo and remains elevated in many DRG neurons for months after nerve injury (Tsujino et al., 2000), one of the principle models of chronic neuropathic pain. Previously, we demonstrated that several injury/stress/RAGs, including ATF3, are increased early (3–4 days) following skin incision (Hill et al., 2010). In the current study we used multiple approaches to determine the time course and extent of skin incision-induced regulation of ATF3 and other injury/stress/RAGs (Table 2). To do this we used real-time qPCR to assess mRNA levels (Fig. 2), and two different immunohistochemical and image analysis approaches to assess protein – a stereological approach to assess the number of neurons expressing genes, and a separate system to assess the relative-intensity of protein expression (Figs. 3 and 4). NPY or GAP-43 mRNA was not examined at the 7-day time point.

3.2.1. ATF3—The transcription factor ATF3 is not normally expressed in adult neurons, but is rapidly induced in response to cellular stress/injury (Tsujino et al., 2000). Expression of ATF3 influences axon growth (Seijffers et al., 2006, 2007), including the growth of afferent pain fibers (Aoki et al., 2007). Early after skin incision (3–4 days), ATF3 is increased in

DRG neurons to a level comparable to that observed following nerve transection (Hill et al., 2010).

To determine if ATF3 expression persisted after incision, ATF3 mRNA was quantified by qPCR of DRG from non-injured rats and rats 4, 7, 14 and 28 DPI. ATF3 mRNA was significantly elevated following skin-incision at all time points examined (Fig. 3A). The level of ATF3 mRNA was highest 4 days following skin incision (~14 fold above control). From 4 to 14 days, ATF3 mRNA levels decreased but then plateaued from 14 to 28 days. Thus is appears that ATF3 mRNA levels increase in DRG following skin incision and although they decrease from the peak they remain elevated long after the skin incision has healed.

To determine the nature of the decrease in ATF3 between 4 and 14 days we addressed whether the decrease was due to a reduction in the number of neurons expressing ATF3 or to a reduction in ATF3 across many/all neurons with little/no change in the number expressing. Stereological image analysis was used to quantify the number of ATF3 expressing neurons within the DRGs 4, 7, 14 and 28 days after incision. The change in the stereologically-estimated total number of $ATF3^+$ neurons over time followed a pattern similar to that of mRNA expression (Fig. 3A). This pattern of expression was maintained when expressing the number of $ATF3^+$ neurons as a proportion of the entire DRG population, with $ATF3^+$ neurons representing 12.9 ± 4.4%, 8.6 ± 4.0%, 4.2 ± 2.2%, 4.5 ± 1.9% of the total DRG neuron population at 4, 7, 14 and 28 DPI, respectively (post-hoc *t*-test indicates $p < 0.001$ versus naïve for all time points). Thus it appears that the reduction of ATF3 mRNA corresponds with a decrease in the number of neurons expressing ATF3 over time.

To determine if ATF3 was expressed in the neurons with axons affected by the incision, the retrograde-tracer DiI was injected into the skin 7 days prior to the incision in a separate set of rats. Expression of ATF3 in DiI-labeled neurons was then assessed at various times after incision of the DiI-injected skin area (control animals had no incision). ATF3 was expressed in the majority of DiI-labeled neurons in the incision animals (72.9%), and less than 0.05% of ATF3-expressing neurons lacked DiI (Fig. 4). Thus, ATF3 appeared to be almost exclusively expressed by neurons with axons projecting to the region of incised skin. Retrograde transport of DiI and expression of ATF3 (for incision rats only) were subsequently used as references for examining the expression and regulation of other genes/markers following incision.

3.2.2. GAP-43—GAP-43 is constitutively expressed in many small/medium-diameter neurons, but not typically in large diameter neurons (Verge et al., 1990; Schreyer and Skene, 1993). After nerve injury GAP-43 expression is upregulated in small/medium neurons and it is expressed de novo in large diameter neurons during axon regeneration (Van der Zee et al., 1989; Verge et al., 1990; Schreyer and Skene, 1993). Previously we demonstrated that GAP-43 mRNA levels increase in the DRG 4 days following skin-incision (Hill et al., 2010). To determine if the increase in GAP-43 expression persisted after incision, GAP-43 mRNA was quantified by qPCR of DRG from non-injured and incision rats. After incision, GAP-43 mRNA levels were slightly elevated but were not significantly different versus non-injured

controls [Non-injured (set to 1): 1.00 ± 0.06; 4 DPI: 1.27 ± 0.12; 14 DPI: 1.33 ± 0.09; 28 DPI: 1.09 ± 0.04; ANOVA p = 0.106].

The lack of difference vs. control in GAP-43 mRNA expression over time could result from the high constitutive expression of GAP-43 and/or because the proportion of DRG neurons responding is small (i.e., low signal-to-noise). However, larger changes could be possible when considering only the ATF3-expressing neurons. To assess the expression of GAP-43 in injured neurons two methods were used. First, those DRG sections prepared for stereological analysis were stained not only for ATF3 (described above), but were also co-labeled for GAP-43 to allow a direct estimation of the number of neurons expressing ATF3 and GAP-43 alone or together. Next, we separately prepared DRG sections from animals that had received DiI injection into their skin followed 7 days later by an incision into the DiI-injection field (controls had no incision), after which the rats survived 7 days and were then euthanized. This was done to determine the effect of incision on the intensity of protein expression.

Both quantitative immunohistochemistry and stereological quantification indicated that there was an increase in the number of DRG neurons expressing GAP-43 following skin incision (Fig. 3A; Table 3). In addition, we determined that most of the $ATF3^+$ neurons were also $GAP\text{-}43^+$. Only a small number of $ATF3^+$ neurons lacked detectible GAP-43. For all time points, the majority of these ATF3-expressing neurons also expressed GAP-43. This includes a notable proportion of the small group of ATF3-expressing large-diameter neurons (particularly at early time points), which do not normally express GAP-43 (Verge et al., 1990) (Table 3). This expression of GAP-43 in large-diameter neurons constitutes a de novo expression, just as occurs after nerve injury.

Next we determined if the incision-induced shift in the population of neurons expressing GAP-43 was accompanied by an increase in the magnitude of GAP-43 expression on a per-neuron basis. The relative intensity of GAP-43 expression within DiI-traced DRG neurons was assessed 7 days after skin-incision (Fig. 4A–F). The intensity of GAP-43 within DiI-labeled neurons was significantly increased throughout the size range of neurons following skin incision (Fig. 4AA; Table 4). Together these multiple approaches indicate that expression of the injury-regulated gene GAP-43 is increased in neurons involved in skin incision.

The discrepancy between the qPCR data and the immunohistochemical data is undoubtedly due to the difference in sensitivity of the techniques to a condition in which the gene-expression changes in a small number of cells occurs against a background of high-expression by many cells. In this situation quantitative histochemistry, in which the cell-by-cell resolution is maintained, is far more sensitive than qPCR of tissue homogenates. Alternatively or concurrently, the level of mRNA may not have changed much at all in the cells that were already expressing it, and protein-production could have been increased through post-translational mechanisms.

3.2.3. NPY—NPY is normally expressed at very low levels by DRG neurons but is one of the most highly-upregulated genes after nerve injury (Wakisaka et al., 1991, 1992; Zhang et

al., 1994; Brumovsky et al., 2004; Tsai et al., 2007). It also appears to be part of a mechanism masking long-lasting hyperalgesia following nerve injury (Solway et al., 2011). To determine if NPY expression is regulated in the DRG following skin-incision, NPY mRNA was quantified by qPCR in DRG from control rats and those receiving skin incision (Fig. 3B). NPY mRNA levels were dramatically-and significantly-increased at all times after incision (Fig. 3B).

To determine if the increase in NPY mRNA in response to skin incision corresponded to an increase in NPY protein expression in injured DRG neurons, we assessed the relative intensity of NPY immunostaining within DiI-traced neurons from control rats and those 7 days after skin-incision (Fig. 4G–L, BB; Table 4). As expected, NPY intensity was low in DRGs from control rats. However, skin incision resulted in an increased NPY relative intensity within small and medium sized DRG neurons. This indicates that skin incision is sufficient to induce NPY expression similar to the regulation which occurs after nerve injury.

3.2.4. CAMK4—To determine if skin incision also leads to persistent downregulation of proteins whose expression is typically decreased by nerve injury, the level of CAMK4 within DRG neurons was examined 7 days following skin-incision. CAMK4 is a regulator of transcription and alternative splicing in neurons (Wayman et al., 2008; Yu et al., 2009). It also has a non-nuclear role and is enriched in small diameter, primarily cutaneous, sensory neurons (Harrison et al., 2014), and is down-regulated by nerve injury (Ji et al., 1996). The intensity of CAMK4 was high in small, medium and large DiI-labeled DRG neurons projecting to the skin in control animals (Fig. 4M–R, CC; Table 4). Following skin incision, CAMK4 staining intensity was reduced by approximately 50% in both small and medium diameter neurons containing DiI and ATF3. Expression and changes in intensity in large diameter neurons was more variable. Thus, skin incision leads to a reduction of CAMK4 expression within DRG neurons projecting to the site of skin incision, consistent with skin incision inducing injury-like responses in DRG neurons. This change was restricted to neurons projecting to the site of incision as non-DiI labeled neurons (not quantified) clearly maintained CAMK4 expression.

3.2.5. IB4—The isolectin B4 (IB4) from *Griffonia simplicifolia* binds to glycoproteins and is used as a marker for a subset of small-to-medium diameter nociceptive neurons (Petruska et al., 1997, 2000, 2002; Fang et al., 2006). Lectin-positive and -negative sensory neurons represent two functionally distinct classes of nociceptors (Molliver et al., 1997; Snider and McMahon, 1998; Stucky and Lewin, 1999) and IB4-binding is reduced in DRG neurons after injury (Bennett et al., 1998). To assess how IB4-binding changes within the DRGs following skin incision IB4-binding was examined via immunohistochemistry 7 days following skin incision. The intensity of IB4-binding was highest in small diameter neurons in DiI-labeled DRGs from control rats with some expression detected in medium sized neurons (Fig 4S–X, DD; Table 4). Following skin-incision the intensity of IB4 staining decreased significantly in DiI-labeled neurons regardless of size. Thus, skin incision leads to a reduction of IB4-binding within DRG neurons projecting to the site of skin incision, consistent with skin incision inducing injury-like responses in DRG neurons. This change

was restricted to neurons projecting to the site of incision as non-DiI labeled neurons (not quantified) clearly maintained IB4-binding.

Taken together, the changes in ATF3, GAP-43, NPY, CAMK4, and IB4-binding suggest that skin incision is sufficient to induce a persistent change in the sensory neurons consistent with that observed following nerve injury.

3.3. Enhanced excitability of sensory neurons traced from incised skin

Peripheral injury-related pain involves the sensory neuron almost necessarily (Reichling et al., 2013). Incision-induced changes in the electrophysiological properties of DRG sensory neurons are correlated with induction and persistence of neuropathic pain (Hämäläinen et al., 2002; Pogatzki et al., 2002b). At the single cell level, neuropathic pain is associated with sensitization of sensory neurons, in which there is a lower threshold for activation (in some cases spontaneous activity is observed). Neuropathic pain is also associated with hyper-responsiveness, which includes changes in the transduction properties of the neurons such that they fire more action potentials and/or fire action potentials at higher frequency, all of which can lead to pathologic pain states if other conditions allow. To determine if the molecular changes observed within the DRG neurons were accompanied by functional changes 28 days after incision, their electrophysiological properties were assessed in acutely-dissociated DRG neurons retrogradely-traced from the incision site or equivalent control skin. Although we measured many electrophysiological properties, most relevant here were the assessments of neuronal excitability (as measured by rheobase) and neuronal responsiveness to sustained stimuli of varying levels of depolarization (action potential metrics).

Only DiI-traced neurons less than 45 um were selected for recording, as this was the population in which the persistent neurochemical effects were most pronounced and most consistently-observed. Because one goal was to determine if any persistent electrophysiological changes might be related to the persistent ATF3-expression, post-hoc immunohistochemistry for ATF3 expression was performed on recorded neurons (Fig. 5A). Importantly, as outlined in the Methods, all recordings were completed well before the dissociation process would have induced ATF3 (Rau et al., 2014), so any ATF3-expression observed in these neurons was due to stress/injury that had occurred in vivo prior to euthanasia and dissociation. Recordings were made from 23 neurons from the incision group and 32 neurons from the control group (tracer-only, no experimental incision), only some of which were successfully recovered for immunohistochemistry. Of the DRG neurons from skin-incision rats successfully recovered for immunocytochemistry, most were ATF3-positive (n = 13/20). Only a minority of those recovered from the control rats were ATF3-positive (n = 9/26; Fig. 5B).

Not all neurons from control animals lacked ATF3. This is not unexpected and was observed in histochemical analyses as well. Because there is precedent for induction of ATF3 by stimuli which may damage axons yet not overtly destroy the skin (Bráz and Basbaum, 2010), it is reasonable to expect that this is most-likely due to axonal damage induced by injection of the tracer. These neurons were included in the analysis to determine if injury induced by tracer injection might affect the neurons. Conversely, not all DiI-traced neurons

from the incision animals expressed ATF3 and likely is due to the tracer spreading into skin regions innervated by axons that are not injured by the incision. According to the histochemical analysis nearly 80% of DiI neurons from incision animals also expressed ATF3. The DiI-traced neurons lacking ATF3 from incision animals provide an excellent, if unintended, control and comparison population which allowed us to determine whether skin incision induced a long-term effect on non-injured neurons that project to the region of the skin incision. Although DiI helped to define the neurons innervating tissue near the incision, the DiI-labeled population was clearly mixed with regard to ATF3-expression. We therefore performed our analyses on data from both the entire population of DiI+ neurons – the standard experimental design in this model – and from DiI-labeled neurons segregated based on ATF3 expression.

3.3.1. Rheobase—Rheobase was used to assess excitability of DiI-labeled neurons with or without skin incision. When considering all DiI+ neurons of each group (i.e., without regard to their ATF3-expression), rheobase is significantly lower in the incision group, suggesting a long-term increase in excitability of sensory neurons induced by skin incision. We also analyzed the results with neurons separated by their ATF3-expression in addition to their incision group. As expected, the greatest difference in rheobase was detected between the ATF3-expressing neurons from incision animals (ostensibly the “true experimental group neurons”) and the ATF3-negative neurons from the control animals (ostensibly the “true control neurons”). Intriguingly, ATF3-positive DRG neurons had a lower rheobase (i.e., were more excitable) than ATF3-negative neurons regardless of skin-incision (Figs. 5C and 6A, Table 5). Further, rheobase did not differ between ATF3-expressing neurons from control and incision animals, nor did rheobase differ between ATF3-negative neurons from control and incision animals. Thus, although skin incision induced an increase in neuronal excitability, ATF3-expression itself, regardless of incision, also acted as a strong discriminator for long-term excitability increases.

3.3.2. Action potential kinetics—In addition to cellular excitability, we also measured responsiveness via two parameters. We assessed the mean spike-rate in response to 1 s depolarizing pulses of different amplitude, with rate expressed as the total number of action potentials fired during the pulse, not considering instantaneous frequency. We also assessed the maximum number of action potentials fired during any depolarizing pulse, regardless of the pulse amplitude.

ATF3-positive neurons had a higher maximum firing rate than ATF3-negative neurons (Fig. 6B) for both control animals and incision animals. Further, maximum action potentials did not differ between ATF3-expressing neurons from control and incision animals, nor did maximum action potentials differ between ATF3-negative neurons from control and incision animals. As we found for rheobase, maximum action potentials were significantly higher in the ATF3-expressing neurons from incision animals when compared to the ATF3-negative neurons from the control animals. However, when considering all neurons of each group (i.e., DiI-labeled but without regard to their ATF3-expression – the standard experimental design for this model), there was no difference between incision and control groups for the maximum number of action potentials (Fig. 6B).

ATF3-positive neurons also had higher mean spike rates than ATF3-negative neurons (Fig. 6C) for both control animals and incision animals. Further, spike rates did not differ between ATF3-expressing neurons from control and incision animals, nor did spike rates differ between ATF3-negative neurons from control and incision animals. As we found for rheobase and maximum action potentials, spike rates were significantly higher in the ATF3-expressing neurons from incision animals when compared to the ATF3-negative neurons from the control animals. When considering all DiI-labeled neurons of each group irrespective of their ATF3-expression (the standard experimental design for this model), there was again no difference between incision and control groups in mean spike rates across all stimulation amplitudes (i.e., without regard to their ATF3-expression; Fig. 6C). Together these data indicate that the hyper-responsive neurons could be discriminated from a mixed population by their expression of ATF3.

No differences were found between groups, or between ATF3-positive neurons and ATF3-negative neurons, for the other electrophysiological parameters assessed (Table 5). Similar to the CTMr observations, we also did not observe any neurons displaying spontaneous activity.

Our electrophysiological assessments support the behavioral and molecular data and demonstrate the existence of a long term cellular injury/stress-like state in neurons induced by skin incision. However, these differences are not detected using only the standard experimental design of recording from DiI-traced neurons, but emerge only when including the additional criterion of ATF3-expression.

4. Discussion

There is a desperate need for the development of preclinical models which more accurately reflect the development of C/PP. To date, the majority of basic science investigations into potential mechanisms of long-term pain after tissue damage focus on damage-induced tissue inflammation and its impact on sensory transduction (Amaya et al., 2013). This is in spite of the fact that one of the hallmarks of chronic neuropathic pain is resistance to anti-inflammatory treatments provided before or during the pain state (Reichling et al., 2013; Sutherland, 2014). In addition, there has been a broad reliance on observing significant effects with the withdrawal reflex in order for new potential mechanisms to be considered feasible and worthy of more in-depth study. This reliance on the withdrawal reflex remains in spite of its significant limitations and work demonstrating that withdrawal reflex-sensitization can be masked in rodents over the same time course as chronic neuropathic pain would develop (Solway et al., 2011; Taylor and Corder, 2014). The number of animal models in which human-like chronic neuropathic pain is observed is far fewer than the number of conditions known to be associated with chronic pain in humans. This is a frustration to researchers, clinicians, and patients alike. It has resulted in a call from the profession to explore new model systems and mechanisms (IOM (U.S.). Committee on Advancing Pain Research Care and Education., 2011; Gereau et al., 2014).

Here we examined the long-term effects of skin incision, a model of surgery and tissue damage which does not involve damage to the gross peripheral nerve. Surgical incision and

tissue damage lead to chronic neuropathic pain in only a proportion of humans but mechanisms underlying this etiology of pain are elusive. Using a nociceptive reflex system with strengths complementing those of the withdrawal reflex system we detected long-term effects of incision. We also pursued potential mechanisms contributing to the behavioral effects from the perspective of sensory neuron cellular-injury/stress, and not necessarily the perspective of tissue-inflammation which has largely ended by 28 days after incision.

Most considerations of the biological processes underlying pain-conditions associated with tissue damage focus on tissue-inflammation and the impact on sensory transduction (Amaya et al., 2013). Because inflammatory mediators can induce electrophysiological sensitization in non-injured neurons (e.g., Fukuoka and Noguchi, 2002; Gold and Flake, 2005) similar to that observed here in injured neurons, sensitization could be due to inflammation of the incised skin as opposed to the neuron-intrinsic injury-response. This is unlikely because the majority of tissue-inflammation appears resolved by 21 DPI (Agaiby and Dyson, 1999; Banik et al., 2005; Kim et al., 2008; Kagawa et al., 2009; Ji et al., 2011; Spofford and Brennan, 2012). Further, if inflammation were involved, 1) one would expect all DiI-labeled neurons would be affected similarly and 2) electrophysiological properties would not be so tightly-linked to ATF3 expression even in non-incision groups. This suggests that the neuron-intrinsic injury response, regardless of the source (i.e., incision, dye-injection, etc.), is the primary factor in establishing the long-lasting electrophysiological sensitization we observe, even if other factors such as inflammation may contribute to some degree. To determine the possible contribution to C/PP of the responses we have described herein it will be necessary to determine if ATF3-expression can be alleviated by standard clinical treatments such as anti-inflammatories and local anesthetics.

Peripheral nerve injury is the single most reliable etiological factor for development of chronic neuropathic pain (Kehlet et al., 2006). Our examination of the effects of skin incision on DRG neurons was from the perspective that tissue damage likely injures sensory axons and induces an intrinsic cellular stress/injury response despite their axons remaining in contact with their target tissue. Some of the same gene regulation induced by nerve injury occurs and persists in sensory neurons innervating incision-associated skin, including de novo expression of ATF3 (Hill et al., 2010) and other stress/injury/regeneration-associated genes. This is true also of degenerating joints (Orita et al., 2011; Ferreira-Gomes et al., 2012), though some of the degenerative models also carry an extended tissue-inflammation component (Orita et al., 2011; Zhang et al., 2013). Interestingly, treatment with adjuvants can also induce expression of ATF3 in sensory neurons (Frezel et al., 2016). This may suggest that inflammation, perhaps via damage to inflamed tissue, might be sufficient to trigger ATF3 expression. Some of the same gene regulation induced by nerve injury occurs and persists in sensory neurons innervating incision-associated skin, and also degenerating joints (Orita et al., 2011; Ferreira-Gomes et al., 2012), though some of the degenerative models also carry an extended tissue-inflammation component (Orita et al., 2011; Zhang et al., 2013). This includes *de novo* expression of ATF3 (Hill et al., 2010) and other stress/injury/regeneration-associated genes. Our examination of the effects of skin incision on DRG neurons was from the perspective that tissue damage likely injures sensory axons and induces an intrinsic cellular stress/injury response despite their axons remaining in contact with their target tissue.

In the current study we determined that genes associated with nerve injury are similarly-affected by skin incision. This is true for genes both upregulated (ATF3, NPY) and downregulated (CAMK4, IB4-binding), and the change in expression persisted for weeks after incision. This suggests maintenance of a neuronal stress/injury response well beyond tissue healing, a response that may be unique to at least some sensory neurons. After sciatic nerve injury, ATF3 expression in spinal sensory neurons continues out to 72 days, the longest time examined, while expression in motoneurons returns to baseline (Tsujino et al., 2000). Sensory neurons thus appear to maintain at least a portion of their response to axonal injury regardless of whether this injury came about from damage to a nerve or to the target tissue (and by extension the axons innervating that tissue).

Histological analysis indicated that the dynamic regulation of ATF3 mRNA over the post-incision time could be accounted for, at least in part, by the number of neurons expressing ATF3. That is, there are clearly fewer neurons of all sizes expressing ATF3 at the later times than the earlier. This does not preclude the possibility that there may also be a change in ATF3 mRNA expressed by individual neurons. It is also unclear if the cells expressing ATF3 at later time points are the same as those expressing ATF3 during the peak of mRNA expression in the whole DRG, though it is reasonable to presume so. It is interesting that the only large-diameter neurons expressing ATF3 at the later times are those which also express GAP-43, another gene expressed de novo in large-diameter DRG neurons. This may suggest a different response to incision in some large-diameter neurons, with one response signified by short-term ATF3 expression without GAP-43, and another by sustained ATF3 and GAP-43 expression. There is precedent for different ATF3 expression patterns in different cells in the same condition (Ohba et al., 2003; Hai et al., 2010; Siebert et al., 2010; Yin et al., 2010). This may be impactful for post-incision sensation because different types of sensory neurons drive different aspects of sensory perception. It will therefore be important to determine whether the transient- vs. persistent-expression of ATF3 follows with cell-type or some other damage-related factor such as proximity to the incision, etc.

The characteristics of the electrophysiological changes suggest potential mechanisms. The major changes were reduced rheobase and increased numbers of action potentials fired in response to depolarization, but not other measures of excitability such as action potential threshold or resting membrane potential, and not action potential properties. Thus, perhaps involvement of T-type voltage-gated Ca^{++} channels (known to regulate action potential bursting behavior; Todorovic and Jevtovic-Todorovic, 2006; Cain and Snutch, 2010) may be more involved than Na^{+} channels which set action potential threshold and many action potential properties (Lai et al., 2004; Chahine and O'Leary, 2014). As far as cellular-electrophysiology may correspond to reflex-behavior, one could expect the properties we recorded to drive a reflex with unchanged threshold but with increased magnitude and duration. The CTMr as implemented here cannot speak to threshold, but did reveal sensitized magnitude/duration. Response-duration has been examined with the Hargreaves test in the past (Ren and Dubner, 1999) but magnitude and duration are generally not measured for withdrawal reflexes. It is therefore understandable that the long-term post-incision sensitization we observed here could have been overlooked thus far.

Post-incision molecular and electrophysiological changes are highly correlated with ATF3-expression, irrespective of experimental group. It remains uncertain how the electrophysiological properties of those neurons with transient ATF3-expression might have been affected. Further, the direct role of ATF3, presumably by regulating transcription, is unclear. The function of ATF3 is context-dependent (Hai et al., 1999), with different cellular temporal and magnitude profiles of ATF3-expression leading to different outcomes after stress/injury, including regulating a cellular survival-or-apoptosis decision point. Thus this unique temporal profile of ATF3 expression in some DRG neurons is intriguing and may be an important clue for understanding how they contribute to sensory pathologies long after the initial insult has resolved.

NPY was also highly upregulated by skin incision, with a temporal pattern of mRNA regulation similar to that described after nerve injury and a cellular distribution selective for ATF3-expressing neurons. NPY-immunoreactivity is extremely low in the non-injured animal, with very few neurons expressing. Peripheral nerve injury produced dramatic increases in the transcription and translation of NPY in large-and medium-diameter DRG neurons (Frisen et al., 1992; Wakisaka et al., 1992; Noguchi et al., 1993), but only rarely in small neurons (Wakisaka et al., 1992; Tsai et al., 2007).

The involvement of NPY may have particular functional importance in relation to persistent pain, and why there are no robust animal models of long-term post-incision pain. Degree of NPY-expression is inversely-correlated with behavioral signs of neuropathic pain (Ruscheweyh et al., 2007). In a limited nerve injury model, NPY acted as an endogenous braking mechanism exerting a tonic and long-lasting inhibitory control of spinal nociceptive transmission, apparently inhibiting the emergence of behavioral signs of chronic pain (Solway et al., 2011). In this model, the delayed administration of NPY receptor antagonists resulted in the “unmasking” of pain-like behaviors, a finding recently replicated in a model of skin incision (Yalamuri et al., 2013) and observed previously with galanin (Hao et al., 1999), another nerve injury-induced neuropeptide upregulated by skin incision (Hill et al., 2010). This indicated that persistent pain-associated changes were subliminally present. The cellular substrate(s) for this masking effect has yet to be identified. The changes we describe here suggest that sensory neurons stressed/injured by tissue damage may be a legitimate substrate for this persistent, yet subliminal, pain-like plasticity. Thus tissue damage – a known etiological factor for C/PP with unknown mechanisms (Kehlet et al., 2006) – induces 1) prolonged sensitization of a no-ciceptive reflex, 2) prolonged sensitization of sensory neurons with ongoing cellular stress/injury response, and 3) prolonged expression of the stress/injury regulator ATF3 and the injury-regulated factor NPY, a molecule capable of suppressing nerve injury-induced pain-behaviors.

5. Conclusions

The full etiological profile of C/PP is unknown, but tissue damage is a major factor. Tissue damage injures and/or stresses sensory axonal endings in the tissue, and this injury/stress phenotype extends to individual cell bodies of the DRG. Sensory neurons innervating damaged tissue express stress/injury/regeneration-associated genes and display electro-physiological and behavioral hypersensitivity similar to that associated with C/PP. These

changes are maintained in some neurons beyond tissue-healing, suggesting that persistent responses may be cell-type-dependent. Expression of ATF3 is highly predictive of which individual sensory neurons display C/PP-related neurochemical and electrophysiological changes, offering a discriminator to use with the mixed population of neurons present in most clinically-relevant models. These data suggest that injury/stress-response processes in single cells may provide a new potential mechanism for the development of C/PP after tissue damage.

Acknowledgments

The authors thank the staff of the KY Spinal Cord Injury Research Center (KSCIRC) for support, particularly Darlene Burke for statistical consultation. This study was supported by the Kentucky Spinal Cord and Head Injury Research Trust (09-12A to JCP, 10-10 to JCP and AGR), the Kentucky Spinal Cord Injury Research Center Traineeship (to KKR), the Burke Foundation (CEH, SBC), Paralyzed Veterans of America Fellowship (#2579 to BJH), NIH (R21NS080091 to JCP and TH, R01NS094741 to JCP), and the Core facilities of the Kentucky Spinal Cord Injury Research Center (P30GM103507 to Scott Whittemore). The authors declare no competing financial interests.

References

Agaiby AD, Dyson M. Immuno-inflammatory cell dynamics during cutaneous wound healing. J Anat. 1999; 195(Pt 4):531–542. [PubMed: 10634692]

Amaya F, Izumi Y, Matsuda M, Sasaki M. Tissue injury and related mediators of pain exacerbation. Curr Neuropharmacol. 2013; 11:592–597. [PubMed: 24396335]

Aoki Y, An HS, Takahashi K, Miyamoto K, Lenz ME, Moriya H, Masuda K. Axonal growth potential of lumbar dorsal root ganglion neurons in an organ culture system: response of nerve growth factor-sensitive neurons to neuronal injury and an inflammatory cytokine. Spine. 2007; 32:857–863. [PubMed: 17426629]

Arroyo-Novoa CM, Figueroa-Ramos MI, Miaskowski C, Padilla G, Stotts N, Puntillo KA. Acute wound pain: gaining a better understanding. Adv Skin Wound Care. 2009; 22:373–380. [PubMed: 19638801]

Banik RK, Subieta AR, Wu C, Brennan TJ. Increased nerve growth factor after rat plantar incision contributes to guarding behavior and heat hyperalgesia. Pain. 2005; 117:68–76. [PubMed: 16061324]

Bennett DL, Michael GJ, Ramachandran N, Munson JB, Averill S, Yan Q, McMahon SB, Priestley JV. A distinct subgroup of small DRG cells express GDNF receptor components and GDNF is protective for these neurons after nerve injury. J Neurosci. 1998; 18:3059–3072. [PubMed: 9526023]

Berge OG. Predictive validity of behavioural animal models for chronic pain. Br J Pharmacol. 2011; 164:1195–1206. [PubMed: 21371010]

Borsook D, Kussman BD, George E, Becerra LR, Burke DW. Surgically induced neuropathic pain: understanding the perioperative process. Ann Surg. 2013; 257:403–412. [PubMed: 23059501]

Bráz JM, Basbaum AI. Differential ATF3 expression in dorsal root ganglion neurons reveals the profile of primary afferents engaged by diverse noxious chemical stimuli. Pain. 2010; 150:290–301. [PubMed: 20605331]

Brennan TJ, Vandermeulen EP, Gebhart GF. Characterization of a rat model of incisional pain. Pain. 1996; 64:493–501. [PubMed: 8783314]

Brumovsky PR, Bergman E, Liu HX, Hokfelt T, Villar MJ. Effect of a graded single constriction of the rat sciatic nerve on pain behavior and expression of immunoreactive NPY and NPY Y1 receptor in DRG neurons and spinal cord. Brain Res. 2004; 1006:87–99. [PubMed: 15047027]

Burgess A, Vigneron S, Brioudes E, Labbe JC, Lorca T, Castro A. Loss of human Greatwall results in G2 arrest and multiple mitotic defects due to deregulation of the cyclin B-Cdc2/PP2A balance. Proc Natl Acad Sci U S A. 2010; 107:12564–12569. [PubMed: 20538976]

Buvanendran A, Kroin JS, Kerns JM, Nagalla SN, Tuman KJ. Characterization of a new animal model for evaluation of persistent postthoracotomy pain. Anesth Analg. 2004; 99:1453–1460. [PubMed: 15502048]

Cain SM, Snutch TP. Contributions of T-type calcium channel isoforms to neuronal firing. Channels. 2010; 4:475–482. [PubMed: 21139420]

Chahine M, O'Leary ME. Regulation/modulation of sensory neuron sodium channels. Handb Exp Pharmacol. 2014; 221:111–135. [PubMed: 24737234]

Chao CY, Ng GY, Cheung KK, Zheng YP, Wang LK, Cheing GL. In vivo and ex vivo approaches to studying the biomechanical properties of healing wounds in rat skin. J Biomech Eng. 2013; 135:101008. [PubMed: 23897434]

Chong MS, Fitzgerald M, Winter J, Hu-Tsai M, Emson PC, Wiese U, Woolf CJ. GAP-43 mRNA in rat spinal cord and dorsal root ganglia neurons: developmental changes and re-expression following peripheral nerve injury. Eur J Neurosci. 1992; 4:883–895. [PubMed: 12106424]

Costigan M, Befort K, Karchewski L, Griffin RS, D'Urso D, Allchorne A, Sitarski J, Mannion JW, Pratt RE, Woolf CJ. Replicate high-density rat genome oligonucleotide micro-arrays reveal hundreds of regulated genes in the dorsal root ganglion after peripheral nerve injury. BMC Neurosci. 2002; 3:16. [PubMed: 12401135]

Davidson S, Copits BA, Zhang J, Page G, Ghetti A, Gereau RW. Human sensory neurons: membrane properties and sensitization by inflammatory mediators. Pain. 2014; 155:1861–1870. [PubMed: 24973718]

de Mos M, Huygen FJ, van der Hoeven-Borgman M, Dieleman JP, Ch Stricker BH, Sturkenboom MC. Outcome of the complex regional pain syndrome. Clin J Pain. 2009; 25:590–597. [PubMed: 19692800]

Djouhri L, Bleazard L, Lawson SN. Association of somatic action potential shape with sensory receptive properties in guinea-pig dorsal root ganglion neurones. J Physiol. 1998; 513(Pt 3):857–872. [PubMed: 9824723]

Ellis A, Bennett DL. Neuroinflammation and the generation of neuropathic pain. Br J Anaesth. 2013; 111:26–37. [PubMed: 23794642]

Fang X, Djouhri L, McMullan S, Berry C, Waxman SG, Okuse K, Lawson SN. Intense isolectin-B4 binding in rat dorsal root ganglion neurons distinguishes C-fiber nociceptors with broad action potentials and high Nav1.9 expression. J Neurosci. 2006; 26:7281–7292. [PubMed: 16822986]

Farahpour MR, Mirzakhani N, Doostmohammadi J, Ebrahimzadeh M. Hydroethanolic *Pistacia atlantica* hulls extract improved wound healing process; evidence for mast cells infiltration, angiogenesis and RNA stability. Int J Surg. 2015; 17:88–98. [PubMed: 25849027]

Ferreira-Gomes J, Adaes S, Sousa RM, Mendonca M, Castro-Lopes JM. Dose-dependent expression of neuronal injury markers during experimental osteoarthritis induced by monoiodoacetate in the rat. Mol Pain. 2012; 8:50. [PubMed: 22769424]

Frezel N, Sohet F, Daneman R, Basbaum AI, Braz JM. Peripheral and central neuronal ATF3 precedes CD4+ T-cell infiltration in EAE. Exp Neurol. 2016; 283(Pt A):224–234. Epub ahead of print. [PubMed: 27343802]

Frisen J, Risling M, Theodorsson E, Fried K. NPY-like immunoreactivity in sensory nerve fibers in rat sciatic neuroma. Brain Res. 1992; 577:142–146. [PubMed: 1521139]

Fukuoka T, Noguchi K. Contribution of the spared primary afferent neurons to the pathomechanisms of neuropathic pain. Mol Neurobiol. 2002; 26:57–67. [PubMed: 12392056]

Gereau RW, Sluka KA, Maixner W, Savage SR, Price TJ, Murinson BB, Sullivan MD, Fillingim RB. A pain research agenda for the 21st century. J Pain. 2014; 15:1203–1214. [PubMed: 25419990]

Goebel A. Complex regional pain syndrome in adults. Rheumatology. 2011; 50:1739–1750. [PubMed: 21712368]

Gold MS, Flake NM. Inflammation-mediated hyperexcitability of sensory neurons. Neurosignals. 2005; 14:147–157. [PubMed: 16215297]

Gong C, Wu Q, Wang Y, Zhang D, Luo F, Zhao X, Wei Y, Qian Z. A biodegradable hydrogel system containing curcumin encapsulated in micelles for cutaneous wound healing. Biomaterials. 2013; 34:6377–6387. [PubMed: 23726229]

Hai T, Wolfgang CD, Marsee DK, Allen AE, Sivaprasad U. ATF3 and stress responses. Gene Expr. 1999; 7:321–335. [PubMed: 10440233]

Hai T, Wolford CC, Chang YS. ATF3, a hub of the cellular adaptive-response network, in the pathogenesis of diseases: is modulation of inflammation a unifying component? Gene Expr. 2010; 15:1–11. [PubMed: 21061913]

Hämäläinen MM, Gebhart GF, Brennan TJ. Acute effect of an incision on mechanosensitive afferents in the plantar rat hindpaw. J Neurophysiol. 2002; 87:712–720. [PubMed: 11826040]

Hao JX, Shi TJ, Xu IS, Kaupilla T, Xu XJ, Hokfelt T, Bartfai T, Wiesenfeld-Hallin Z. Intrathecal galanin alleviates allodynia-like behaviour in rats after partial peripheral nerve injury. Eur J Neurosci. 1999; 11:427–432. [PubMed: 10051743]

Harrison BJ, Flight RM, Gomes C, Venkat G, Ellis SR, Sankar U, Twiss JL, Rouchka EC, Petruska JC. IB4-binding sensory neurons in the adult rat express a novel 3′ UTR-extended isoform of CaMK4 that is associated with its localization to axons. J Comp Neurol. 2014; 522:308–336. [PubMed: 23817991]

Hill CE, Harrison BJ, Rau KK, Hougland MT, Bunge MB, Mendell LM, Petruska JC. Skin incision induces expression of axonal regeneration-related genes in adult rat spinal sensory neurons. J Pain. 2010; 11:1066–1073. [PubMed: 20627820]

Huge V, Lauchart M, Magerl W, Beyer A, Moehnle P, Kaufhold W, Schelling G, Azad SC. Complex interaction of sensory and motor signs and symptoms in chronic CRPS. PLoS One. 2011; 6:e18775. [PubMed: 21559525]

Institute of Medicine (U.S.). Committee on Advancing Pain Research Care and Education. Relieving Pain in America: A Blueprint for Transforming Prevention, Care, Education, and Research. National Academies Press; Washington, D.C: 2011R.

Ji RR, Shi TJ, Xu ZQ, Zhang Q, Sakagami H, Tsubochi H, Kondo H, Hokfelt T. Ca^{2+}/calmodulin-dependent protein kinase type IV in dorsal root ganglion: colocalization with peptides, axonal transport and effect of axotomy. Brain Res. 1996; 721:167–173. [PubMed: 8793097]

Ji RR, Xu ZZ, Strichartz G, Serhan CN. Emerging roles of resolvins in the resolution of inflammation and pain. Trends Neurosci. 2011; 34:599–609. [PubMed: 21963090]

Jiang N, Rau KK, Johnson RD, Cooper BY. Proton sensitivity Ca^{2+} permeability and molecular basis of acid-sensing ion channels expressed in glabrous and hairy skin afferents. J Neurophysiol. 2006; 95:2466–2478. [PubMed: 16407431]

Kagawa S, Matsuo A, Yagi Y, Ikematsu K, Tsuda R, Nakasono I. The time-course analysis of gene expression during wound healing in mouse skin. Leg Med (Tokyo). 2009; 11:70–75. [PubMed: 18974019]

Kang S, Lee D, Theusch BE, Arpey CJ, Brennan TJ. Wound Hypoxia in Deep Tissue After Incision in Rats. Wound Repair and Regeneration: Official Publication of the Wound Healing Society [and] the European Tissue Repair Society. 2013; 21:730–739.

Kehlet H, Jensen TS, Woolf CJ. Persistent postsurgical pain: risk factors and prevention. Lancet. 2006; 367:1618–1625. [PubMed: 16698416]

Kim MH, Liu W, Borjesson DL, Curry FR, Miller LS, Cheung AL, Liu FT, Isseroff RR, Simon SI. Dynamics of neutrophil infiltration during cutaneous wound healing and infection using fluorescence imaging. J Invest Dermatol. 2008; 128:1812–1820. [PubMed: 18185533]

Lai J, Porreca F, Hunter JC, Gold MS. Voltage-gated sodium channels and hyperalgesia. Annu Rev Pharmacol Toxicol. 2004; 44:371–397. [PubMed: 14744251]

Lokmic Z, Darby IA, Thompson EW, Mitchell GM. Time Course Analysis of Hypoxia, Granulation Tissue and Blood Vessel Growth, and Remodeling in Healing Rat Cutaneous Incisional Primary Intention Wounds. Wound Repair and Regeneration: Official Publication of the Wound Healing Society [and] the European Tissue Repair Society. 2006; 14:277–288.

Ma C, Shu Y, Zheng Z, Chen Y, Yao H, Greenquist KW, White FA, LaMotte RH. Similar electrophysiological changes in axotomized and neighboring intact dorsal root ganglion neurons. J Neurophysiol. 2003; 89:1588–1602. [PubMed: 12612024]

Mogil JS, Davis KD, Derbyshire SW. The necessity of animal models in pain research. Pain. 2010; 151:12–17. [PubMed: 20696526]

Molliver DC, Wright DE, Leitner ML, Parsadanian AS, Doster K, Wen D, Yan Q, Snider WD. IB4-binding DRG neurons switch from NGF to GDNF dependence in early post-natal life. Neuron. 1997; 19:849–861. [PubMed: 9354331]

Noguchi K, De Leon M, Nahin RL, Senba E, Ruda MA. Quantification of axotomy-induced alteration of neuropeptide mRNAs in dorsal root ganglion neurons with special reference to neuropeptide Y mRNA and the effects of neonatal capsaicin treatment. J Neurosci Res. 1993; 35:54–66. [PubMed: 7685398]

Ohba N, Maeda M, Nakagomi S, Muraoka M, Kiyama H. Biphasic expression of activating transcription factor-3 in neurons after cerebral infarction. Brain Res Mol Brain Res. 2003; 115:147–156. [PubMed: 12877985]

Orita S, Ishikawa T, Miyagi M, Ochiai N, Inoue G, Eguchi Y, Kamoda H, Arai G, Toyone T, Aoki Y, Kubo T, Takahashi K, Ohtori S. Pain-related sensory innervation in monoiodoacetate-induced osteoarthritis in rat knees that gradually develops neuronal injury in addition to inflammatory pain. BMC Musculoskelet Disord. 2011; 12:134. [PubMed: 21679434]

Perkins FM, Kehlet H. Chronic pain as an outcome of surgery. A review of predictive factors. Anesthesiology. 2000; 93:1123–1133. [PubMed: 11020770]

Petruska JC, Barker DF, Garraway SM, Trainer R, Fransen JW, Seidman PA, Soto RG, Mendell LM, Johnson RD. Organization of sensory input to the nociceptive-specific cutaneous trunk muscle reflex in rat, an effective experimental system for examining nociception and plasticity. J Comp Neurol. 2014; 522:1048–1071. [PubMed: 23983104]

Petruska JC, Napaporn J, Johnson RD, Cooper BY. Chemical responsiveness and histochemical phenotype of electrophysiologically classified cells of the adult rat dorsal root ganglion. Neuroscience. 2002; 115:15–30. [PubMed: 12401318]

Petruska JC, Napaporn J, Johnson RD, Gu JG, Cooper BY. Subclassified acutely dissociated cells of rat DRG: histochemistry and patterns of capsaicin-, proton-, and ATP-activated currents. J Neurophysiol. 2000; 84:2365–2379. [PubMed: 11067979]

Petruska JC, Streit WJ, Johnson RD. Localization of unmyelinated axons in rat skin and mucocutaneous tissue utilizing the isolectin GS-I-B4. Somatosens Mot Res. 1997; 14:17–26. [PubMed: 9241725]

Pogatzki EM, Niemeier JS, Brennan TJ. Persistent secondary hyperalgesia after gastrocnemius incision in the rat. Eur J Pain. 2002a; 6:295–305. [PubMed: 12161095]

Pogatzki EM, Vandermeulen EP, Brennan TJ. Effect of plantar local anesthetic injection on dorsal horn neuron activity and pain behaviors caused by incision. Pain. 2002b; 97:151–161. [PubMed: 12031788]

Rau KK, Jiang N, Johnson RD, Cooper BY. Heat sensitization in skin and muscle nociceptors expressing distinct combinations of TRPV1 and TRPV2 protein. J Neurophysiol. 2007; 97:2651–2662. [PubMed: 17287441]

Rau KK, Petruska JC, Cooper BY, Johnson RD. Distinct subclassification of DRG neurons innervating the distal colon and glans penis/distal urethra based on the electrophysiological current signature. J Neurophysiol. 2014; 112:1392–1408. [PubMed: 24872531]

Reichling DB, Green PG, Levine JD. The fundamental unit of pain is the cell. Pain. 2013; 154(Suppl 1)

Ren K, Dubner R. Inflammatory models of pain and hyperalgesia. ILAR J. 1999; 40:111–118. [PubMed: 11406689]

Ruscheweyh R, Forsthuber L, Schoffnegger D, Sandkuhler J. Modification of classical neurochemical markers in identified primary afferent neurons with Abeta-, Adelta-, and C-fibers after chronic constriction injury in mice. J Comp Neurol. 2007; 502:325–336. [PubMed: 17348016]

Schreyer DJ, Skene JH. Injury-associated induction of GAP-43 expression displays axon branch specificity in rat dorsal root ganglion neurons. J Neurobiol. 1993; 24:959–970. [PubMed: 8228973]

Seijffers R, Allchorne AJ, Woolf CJ. The transcription factor ATF-3 promotes neurite outgrowth. Mol Cell Neurosci. 2006; 32:143–154. [PubMed: 16713293]

Seijffers R, Mills CD, Woolf CJ. ATF3 increases the intrinsic growth state of DRG neurons to enhance peripheral nerve regeneration. J Neurosci. 2007; 27:7911–7920. [PubMed: 17652582]

Siebert JR, Middleton FA, Stelzner DJ. Long descending cervical propriospinal neurons differ from thoracic propriospinal neurons in response to low thoracic spinal injury. BMC Neurosci. 2010; 11:148. [PubMed: 21092315]

Siegel, S.; Castellan, J. Nonparametric Statistics for the Behavioral Sciences. 2. McGraw Hill; Boston: 1988.

Snider WD, McMahon SB. Tackling pain at the source: new ideas about nociceptors. Neuron. 1998; 20:629–632. [PubMed: 9581756]

Solway B, Bose SC, Corder G, Donahue RR, Taylor BK. Tonic inhibition of chronic pain by neuropeptide Y. Proc Natl Acad Sci U S A. 2011; 108:7224–7229. [PubMed: 21482764]

Soybir OC, Gurdal SO, Oran ES, Tulubas F, Yuksel M, Akyildiz AI, Bilir A, Soybir GR. Delayed cutaneous wound healing in aged rats compared to younger ones. Int Wound J. 2012; 9:478–487. [PubMed: 22128764]

Spofford CM, Brennan TJ. Gene expression in skin, muscle, and dorsal root ganglion after plantar incision in the rat. Anesthesiology. 2012; 117:161–172. [PubMed: 22617252]

Stucky CL, Lewin GR. Isolectin B(4)-positive and -negative nociceptors are functionally distinct. J Neurosci. 1999; 19:6497–6505. [PubMed: 10414978]

Sutherland S. Pain that won't quit. Sci Am. 2014; 311(60–65):67.

Taylor BK, Corder G. Endogenous analgesia, dependence, and latent pain sensitization. Curr Top Behav Neurosci. 2014; 20:283–325. [PubMed: 25227929]

Todorovic SM, Jevtovic-Todorovic V. The role of T-type calcium channels in peripheral and central pain processing. CNS Neurol Disord Drug Targets. 2006; 5:639–653. [PubMed: 17168748]

Tsai YJ, Lin CT, Lue JH. Characterization of the induced neuropeptide Y-like immunoreactivity in primary sensory neurons following complete median nerve transection. J Neurotrauma. 2007; 24:1878–1888. [PubMed: 18159999]

Tsujino H, Kondo E, Fukuoka T, Dai Y, Tokunaga A, Miki K, Yonenobu K, Ochi T, Noguchi K. Activating transcription factor 3 (ATF3) induction by axotomy in sensory and motoneurons: a novel neuronal marker of nerve injury. Mol Cell Neurosci. 2000; 15:170–182. [PubMed: 10673325]

Van der Zee CE, Nielander HB, Vos JP, Lopes da Silva S, Verhaagen J, Oestreicher AB, Schrama LH, Schotman P, Gispen WH. Expression of growth-associated protein B-50 (GAP-43) in dorsal root ganglia and sciatic nerve during regenerative sprouting. J Neurosci. 1989; 9:3505–3512. [PubMed: 2552034]

Verge VM, Tetzlaff W, Richardson PM, Bisby MA. Correlation between GAP-43 and nerve growth factor receptors in rat sensory neurons. J Neurosci. 1990; 10:926–934. [PubMed: 2156965]

Vierck CJ, Yezierski RP. Comparison of operant escape and reflex tests of nociceptive sensitivity. Neurosci Biobehav Rev. 2015; 51:223–242. [PubMed: 25660956]

Wakisaka S, Kajander KC, Bennett GJ. Increased neuropeptide Y (NPY)-like immunoreactivity in rat sensory neurons following peripheral axotomy. Neurosci Lett. 1991; 124:200–203. [PubMed: 1712437]

Wakisaka S, Kajander KC, Bennett GJ. Effects of peripheral nerve injuries and tissue inflammation on the levels of neuropeptide Y-like immunoreactivity in rat primary afferent neurons. Brain Res. 1992; 598:349–352. [PubMed: 1486499]

Wayman GA, Lee YS, Tokumitsu H, Silva AJ, Soderling TR. Calmodulin-kinases: modulators of neuronal development and plasticity. Neuron. 2008; 59:914–931. [PubMed: 18817731]

Woolf CJ, Salter MW. Neuronal plasticity: increasing the gain in pain. Science. 2000; 288:1765–1769. [PubMed: 10846153]

Yalamuri SM, Brennan TJ, Spofford CM. Neuropeptide Y is analgesic in rats after plantar incision. Eur J Pharmacol. 2013; 698:206–212. [PubMed: 23123350]

Yin X, Wolford CC, Chang YS, McConoughey SJ, Ramsey SA, Aderem A, Hai T. ATF3, an adaptive-response gene, enhances TGF{beta} signaling and cancer-initiating cell features in breast cancer cells. J Cell Sci. 2010; 123:3558–3565. [PubMed: 20930144]

Yu J, Hai Y, Liu G, Fang T, Kung SK, Xie J. The heterogeneous nuclear ribonucleoprotein L is an essential component in the Ca^{2+}/calmodulin-dependent protein kinase IV-regulated alternative

splicing through cytidine-adenosine repeats. J Biol Chem. 2009; 284:1505–1513. [PubMed: 19017650]

Zhang RX, Ren K, Dubner R. Osteoarthritis pain mechanisms: basic studies in animal models. Osteoarthr Cartil. 2013; 21:1308–1315. [PubMed: 23973145]

Zhang X, Wiesenfeld-Hallin Z, Hokfelt T. Effect of peripheral axotomy on expression of neuropeptide Y receptor mRNA in rat lumbar dorsal root ganglia. Eur J Neurosci. 1994; 6:43–57. [PubMed: 8130932]

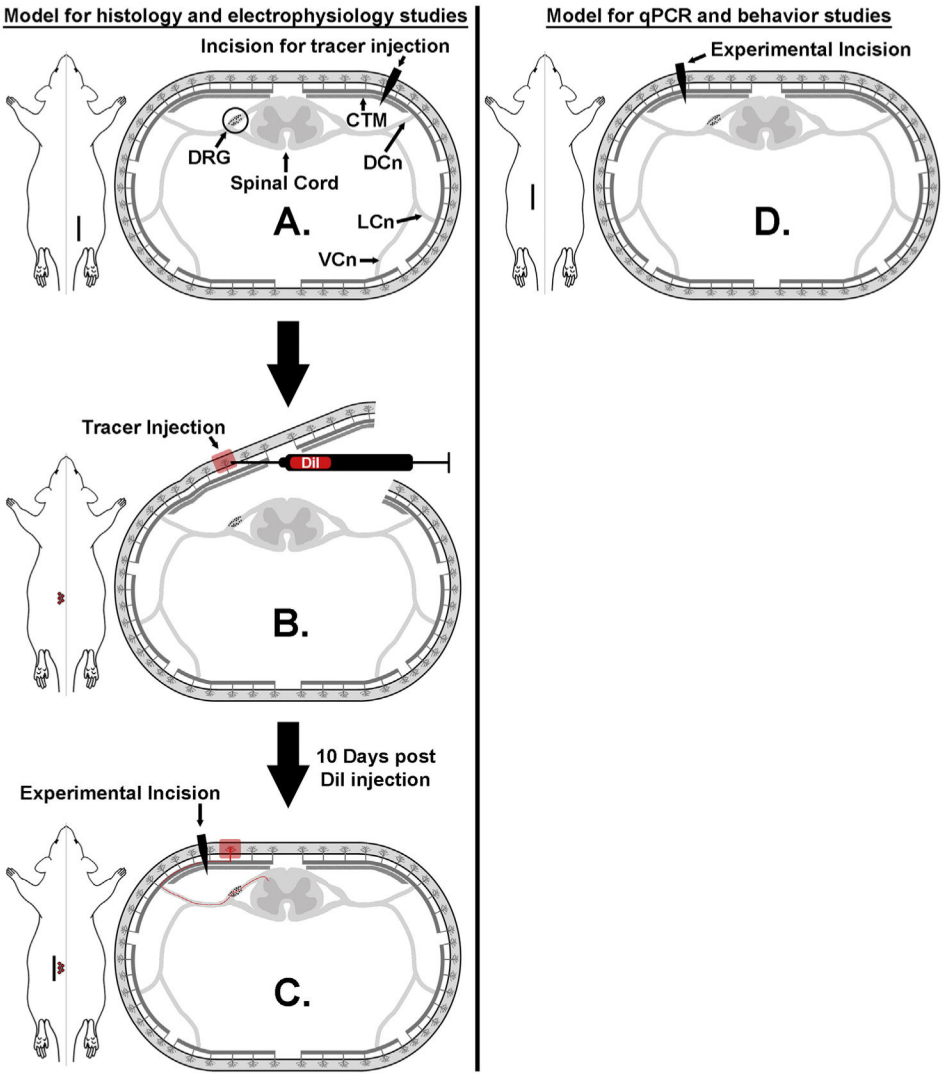

Fig. 1.

Schematic diagrams of skin incision as a model of tissue injury. Animal models used for histology/electrophysiology (A–C) and qPCR/behavior (D) are shown. Sites of skin incision and DiI injection in relation to the dorsal root ganglion (DRG), cutaneous trunci muscle (CTM), and dorsal (DCn), lateral (LCn) and ventral (VCn) cutaneous nerves are indicated in D. In the histology/electrophysiology studies, an initial skin incision was made through the hairy skin (A) to allow DiI injections into the contralateral skin (B). Ten days later, the experimental incision was made immediately lateral to the site of DiI injection (C). For the qPCR/behavior studies (D), a single incision was made through the hairy skin.

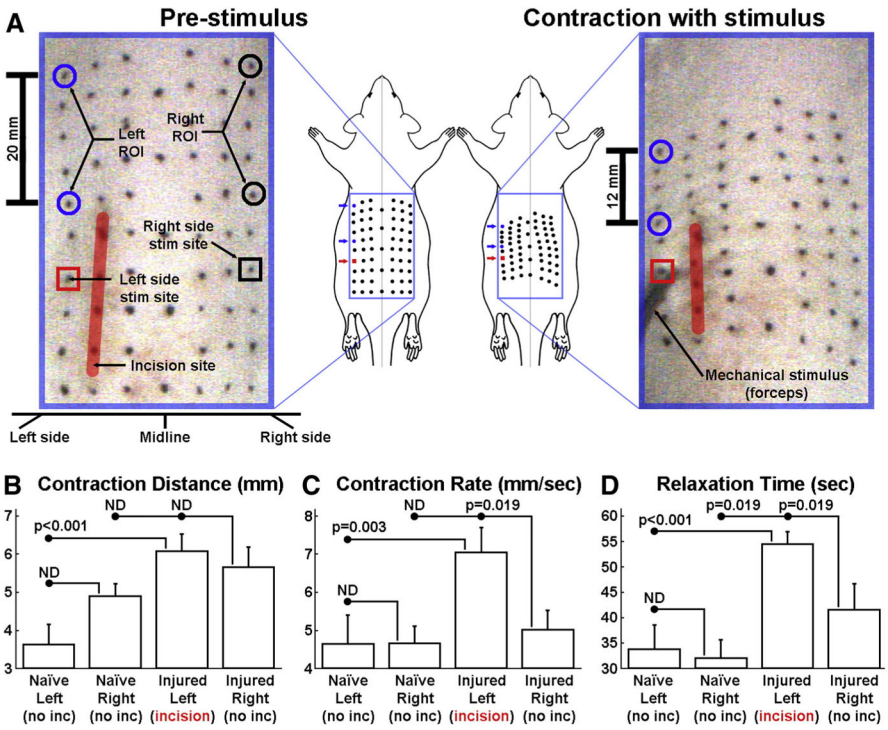

Fig. 2.

Skin incision induces long-term sensitization of a nociceptive reflex. Schematic shows key aspects of CTMr biokinematics (A). Mechanical pinch is applied to the skin (red square) adjacent to the incision site (red line). Movement of the dots is quantified rostral to the stimulus site (blue circles; focus of CTMr is 1 mm rostral to stimulus). Mean contraction distance (B), contraction rate (C), and post-stimulus relaxation time (D), are shown for the regions of interest (blue circles in A), in control and skin incised animals (n = 4 animals per group; 28 DPI). Error bars are SEM; significance determined by ANOVA. (For interpretation of the references to colour in this figure legend, the reader is referred to the web version of this article.)

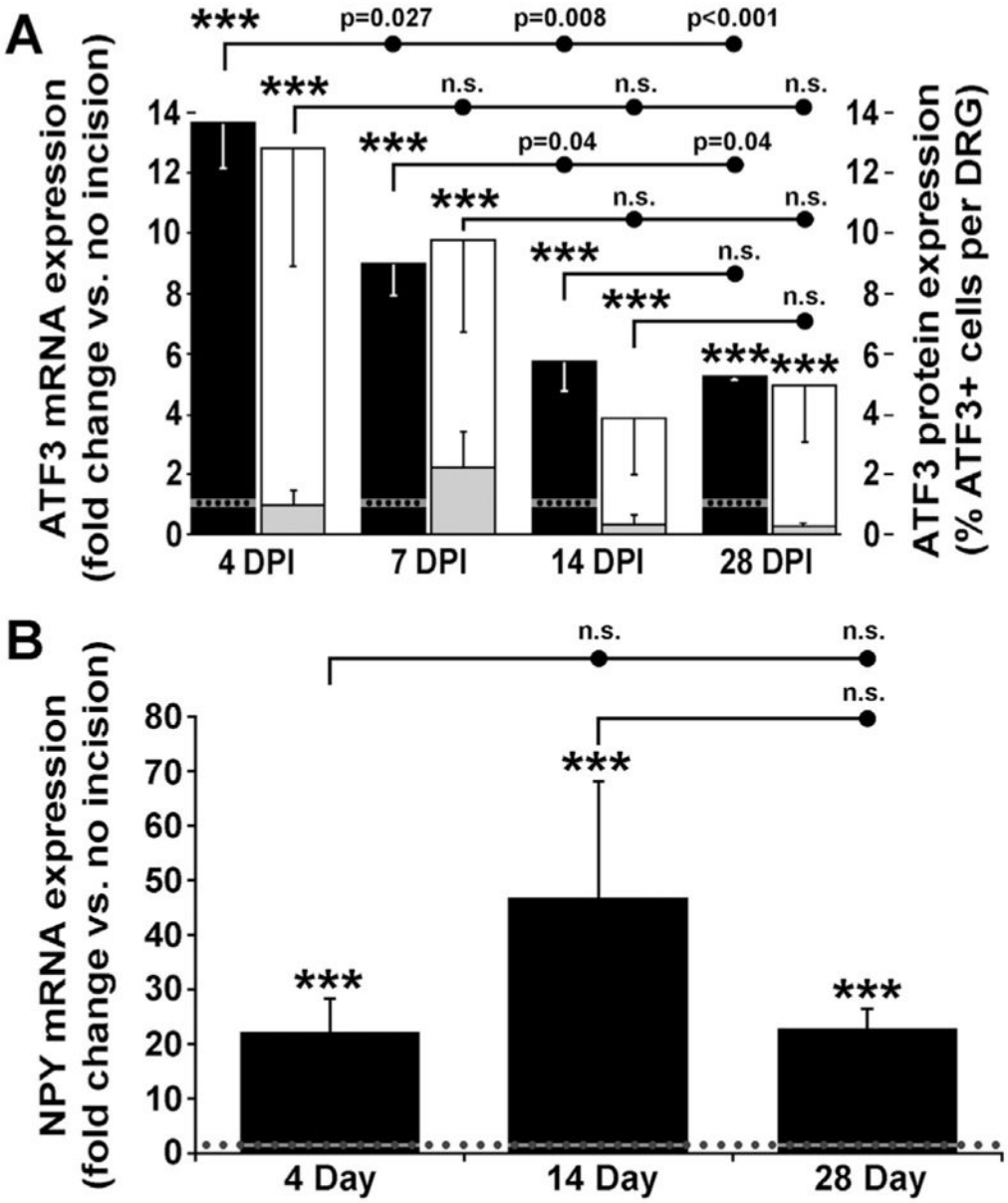

Fig. 3.

Molecular assessment of the expression of stress/injury-regulated genes. ATF3 expression (A) by qPCR (y-axis on left, black bars) and by IHC (y-axis on right, white/gray bars) in DRG housing neurons serving incised skin at various days post incision (DPI). ATF3 in control DRG is essentially absent, and is set to "1" (dotted line; refers to qPCR). Total percentage of $ATF3^+$ cells per injured DRG (y-axis on right) is depicted *with* (white bars) and *without* (gray bars) GAP-43 co-expression. NPY mRNA expression (B) is also shown for time points relative to non-incised control level (dotted lines). Asterisks indicate significant difference versus uninjured control by ANOVA [$p < 0.001$ (***)]. Lines above bars indicate the statistical analyses for each time point compared to the others. Error bars are SEM. Non-injured controls are set to 1.00 fold change, and ±SEM is indicated by a gray

bar behind the black dotted line, which is ±0.19 for ATF3 and ±0.20 for NPY. n.s. = not significant.

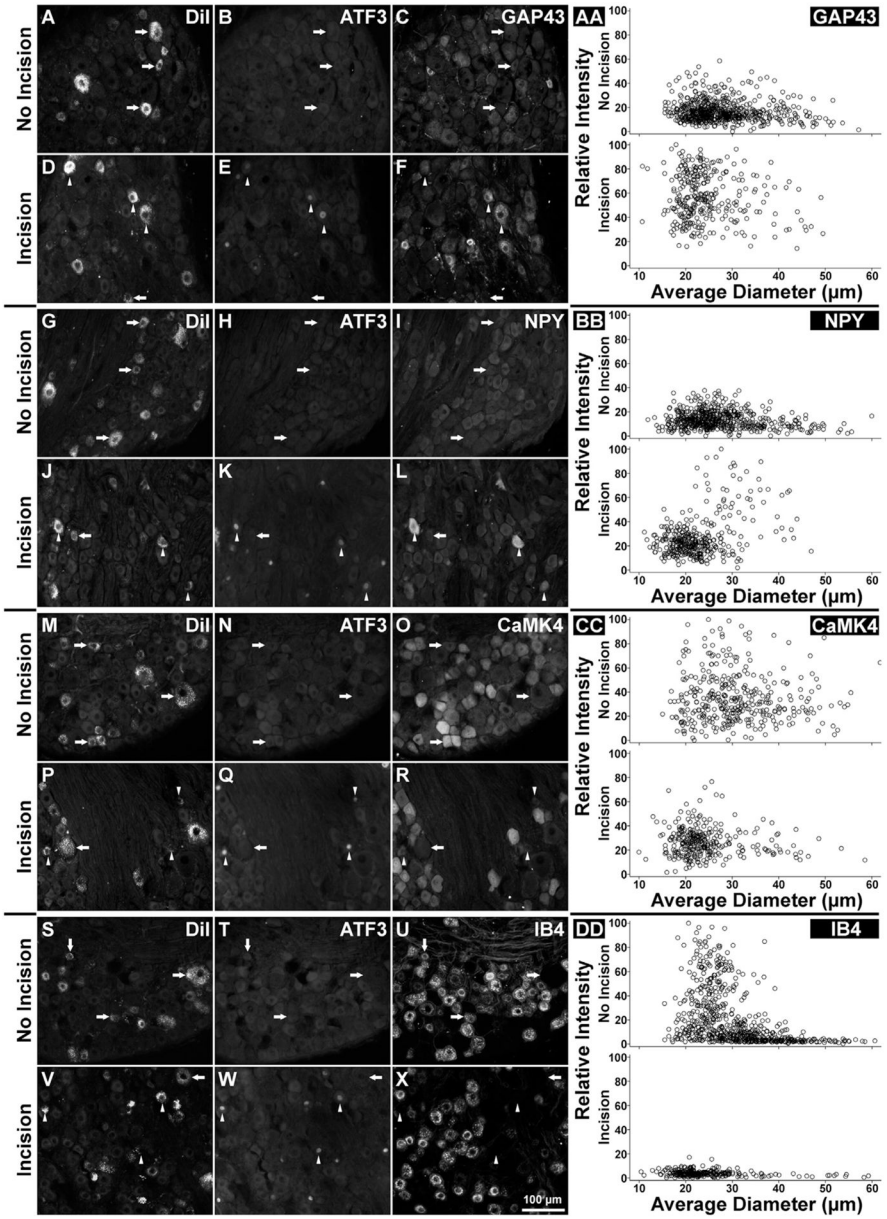

Fig. 4.

Immunohistochemical detection of ATF3 and other cellular stress/injury markers after skin incision. Examples of protein expression of ATF3 (B, E, H, K, N, Q, T, W), GAP-43 (C, F), NPY (I, L) and CAMK4 (O, R), and IB4-binding (U, X) is shown in sectioned DRG, for control group and 7 DPI. Arrows indicate DiI+ neurons (A, D, G, J, M, P, S, V) that *do not* express ATF3. Arrowheads indicate DiI+ neurons that co-express ATF3. Scatterplots showing the relative intensities (arbitrary scale, normalized to a scale of 100) versus average cell diameter are shown for every cell analyzed for GAP-43, NPY, and CAMK4 expression, and IB4-binding (AA, BB, CC, and DD, respectively). Scale bar for all images is located in panel X. Refer also to Table 4.

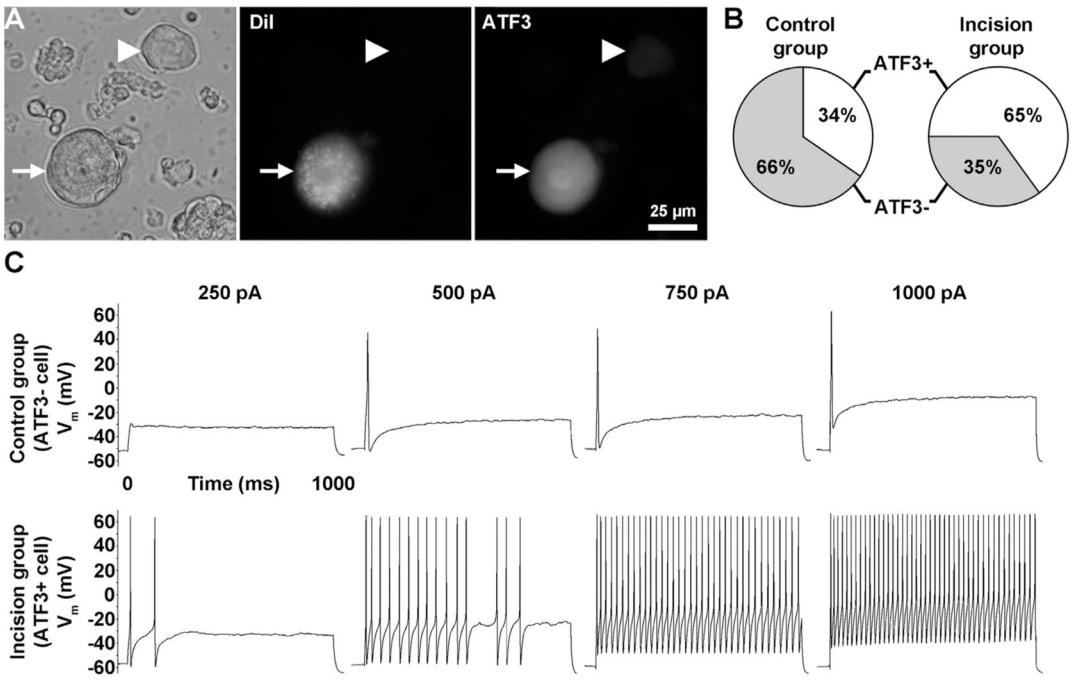

Fig. 5.

Electrophysiological recordings from DRG neurons retrogradely traced from the back hairy skin of control non-incised animals and from those with skin incision. An example of a recorded neuron is shown (A), including brightfield view (left panel), as well as fluorescent views of DiI labeling (center panel) and ATF3 immunoreactivity (right panel). Scale bar for all images is located in the right panel. Percent population of ATF3 immunoreactivity for control and skin-incised animals (B), as well as examples of the action potentials evoked by increasing current stimuli (250, 500, 750 and 1000 pA; all 1000 ms duration) are shown for a control ATF3-negative neuron and an incised ATF3-positive neuron (C).

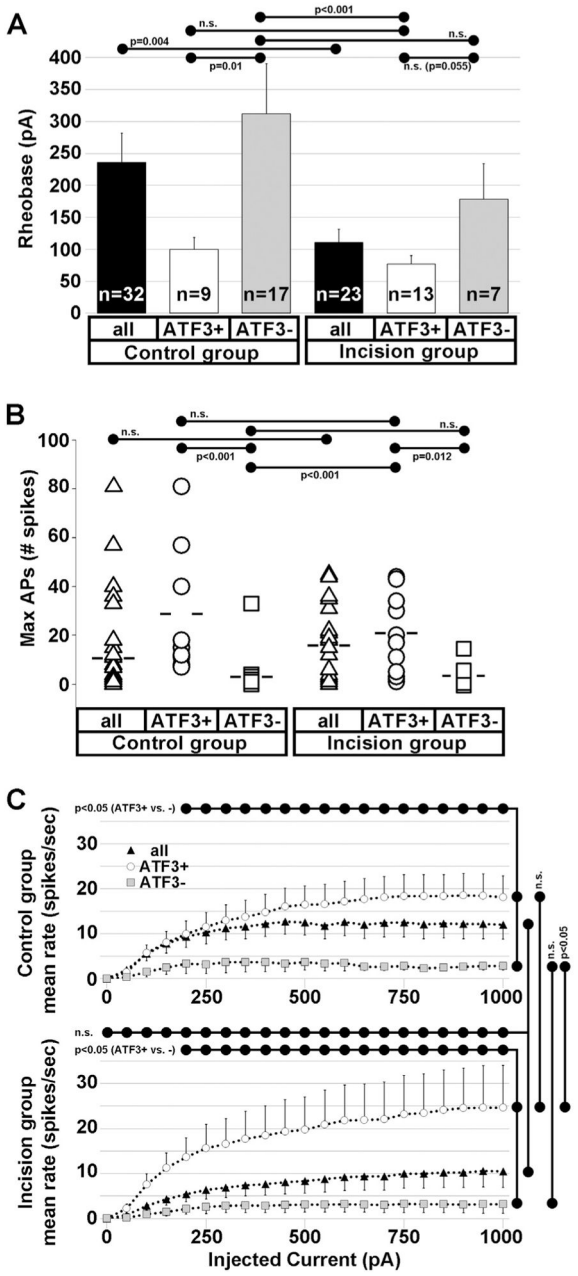

Fig. 6.

Electrophysiological characteristics of recorded DRG neurons retrogradely traced from the back hairy skin of control and skin-incised animals. Data are from all neurons recorded from control and incision animals (group comparison, indicated as “all”), as well as subsets of neurons from each of these groups segregated based on ATF3 immunoreactivity. Rheobase (A), maximum number of action potentials evoked for each recorded neuron regardless of stimulus intensity (B), and mean action potential spike rate for each stimulus intensity (C), are shown. Relationships between groups are indicated with bars. Differences are indicated

by p value or n.s. (no significance). All error bars indicate SEM; significance determined by ANOVA. Refer also to Table 5.

Table 1

Details of primers used for qPCR assays.

Gene	Accession #	Forward primer (5′–3′)	Tm (°C)	Reverse primer (5′–3′)	Tm (°C)
GAPDH	NP_058704	ATGGCCTTCCGTGTTCCTAC	65.00	AGACAACCTGGTCCTCCTCAGTG	61.90
ATF3	NP_037044	GAGATGTCAGTCACCAAGTC	60.05	TTCTTCAGCTCCTCGATCTG	61.36
GAP-43	NP_058891	CTAAACAAGCCGATGTGCC	63.20	TTCTTTACCCTCATCCTGTCG	62.90
NPY	NP_036746	CAGACAGAGATATGGCAAGAG	59.98	GAGAGCAAGTTTCATTTCCC	59.12

Table 2

Organization of assessments. Each assessment/column used separate samples, but assessments within each column were made from the same samples.

		Protein	
	mRNA	Number	Intensity
	4–28 d	4–28 d	7 d
ATF3	X	X	
GAP-43	X	X	X
NPY	X		X
CAMK4			X
IB4			X

Table 3

Stereological analysis of ATF3 protein expression in DRG in uninjured control animals and in animals 4, 7, 14 and 28 days after skin incision. Data set for Fig. 3A is shown. Populations are divided between ATF3-expressing neurons that co-express (top rows) or do not co-express (bottom rows) GAP-43. Cell diameter is classified as Small (<30 μm), Medium (30–45 μm) and Large (>45 μm), and the proportion of $ATF3^+$ neurons in each group for the indicated timepoint is provided. Independent *t*-tests were used to determine significance of incised versus control group.

Population	Time point	Estimated mean # cells in DRG	Estimated mean % cells in DRG	p value	% small	% medium	% large
$ATF3^+$ $GAP\text{-}43^+$	Non-incised	4 ± 4	0.0 ± 0.0	–	100.00	0.00	0.00
	4 DPI	980 ± 322	11.9 ± 4.0	<0.001	86.48	12.30	1.23
	7 DPI	620 ± 311	7.5 ± 3.1	<0.001	92.86	6.49	0.65
	14 DPI	300 ± 186	3.5 ± 1.9	<0.001	94.44	5.56	0.00
	28 DPI	328 ± 113	4.7 ± 1.9	<0.001	83.95	13.58	2.47
$ATF3^+$ $GAP\text{-}43^-$	Non-incised	12 ± 8	0.1 ± 0.1	–	0.00	100.00	0.00
	4 DPI	76 ± 39	1.0 ± 0.5	<0.001	61.11	16.67	22.22
	7 DPI	176 ± 88	2.3 ± 1.1	<0.001	90.91	6.82	2.27
	14 DPI	32 ± 27	0.4 ± 0.3	<0.001	85.71	14.29	0.00
	28 DPI	23 ± 9	0.3 ± 0.1	<0.001	83.33	16.67	0.00

Table 4

Relative-intensity of immunolabeling in DRG neurons from control non-incised rats and from rats with skin incision (7 DPI). The same data set shown in Fig. 4 is analyzed here. Cell diameter is defined as small (<30 μm), medium (30–45 μm) and large (>45 μm). ANOVA indicated significant differences existed between groups ($p < 0.001$). Where applicable, *t*-tests were used to determine if the difference between the control and incision groups reached significance ("p-value" column). The range of mean fluorescence intensity of each neuron was normalized to a scale of 0–100 for each marker, regardless of cell size or group. Intensity values are listed as the average ± SEM, followed by the total number of cells per group in parentheses.

IHC marker	Cell diameter	Control group mean intensity	Incision group mean intensity	p value
GAP-43	Small	17.31 ± 0.40 (446)	57.92 ± 1.17 (268)	<0.001
	Medium	16.19 ± 0.67 (171)	52.26 ± 2.81 (49)	<0.001
	Large	10.82 ± 1.45 (20)	35.22 ± 4.81 (5)	<0.001
NPY	Small	14.05 ± 0.33 (439)	24.33 ± 0.78 (330)	<0.001
	Medium	12.16 ± 0.58 (136)	44.85 ± 3.84 (42)	<0.001
	Large	7.29 ± 0.91 (22)	15.42 ± 0.00 (1)	NA
CaMK4	Small	36.44 ± 1.59 (192)	26.92 ± 0.73 (266)	<0.001
	Medium	33.46 ± 1.51 (145)	24.59 ± 1.47 (40)	0.002
	Large	32.23 ± 3.65 (27)	19.18 ± 3.41 (4)	0.149
IB4	Small	30.49 ± 1.34 (353)	4.04 ± 0.14 (252)	<0.001
	Medium	9.85 ± 0.79 (265)	2.78 ± 0.34 (25)	<0.001
	Large	2.74 ± 0.24 (40)	1.75 ± 0.24 (10)	0.014

Table 5

Electrophysiological and cellular properties of recorded DRG neurons retrogradely traced from the back hairy skin of control and skin-incised animals. Data set for Fig. 6 is shown. Groups include all neurons recorded from control and skin-incised animals, as well as subsets from each of these groups after testing for ATF3 immunoreactivity.

	Group	n (# cells)	Average cell diameter (μm)	Capacitance (pF)	RMP (mV)	AHP80 (ms)	AHP ampl. (mV)	AP threshold (−mV)	AP duration (ms)	Rheobase (pA)
Control group	All	32	35.4 ± 0.8	63.6 ± 4.3	49.1 ± 1.1	142.2 ± 17.9	9.7 ± 0.8	17.1 ± 1.5	4.0 ± 0.5	235.9 ± 46.1
	$ATF3^+$	9	35.5 ± 1.7	63.4 ± 7.5	52.3 ± 1.9	138.1 ± 28.8	10.5 ± 1.6	20.8 ± 3.5	4.5 ± 1.4	100.0 ± 18.6
	$ATF3^-$	17	35.4 ± 1.2	65.9 ± 7.0	48.5 ± 1.4	158.9 ± 28.0	9.5 ± 1.0	15.4 ± 1.9	4.1 ± 0.4	311.8 ± 79.0
Incised group	All	23	34.9 ± 1.0	58.2 ± 3.9	46.6 ± 1.7	117.4 ± 11.6	9.7 ± 1.5	16.2 ± 2.2	3.9 ± 0.4	110.9 ± 20.4
	$ATF3^+$	13	35.6 ± 1.3	58.0 ± 4.1	47.1 ± 2.7	120.6 ± 16.4	9.9 ± 2.2	18.5 ± 3.0	3.8 ± 0.6	76.9 ± 13.4
	$ATF3^-$	7	35.2 ± 1.2	63.1 ± 8.8	47.5 ± 1.6	126.9 ± 15.4	6.6 ± 1.3	17.8 ± 3.3	3.9 ± 0.7	178.6 ± 55.5